REVIEW

Binary and Ternary Atomic Layers Built from Carbon, Boron, and Nitrogen

*Li Song, Zheng Liu, Arava Leela Mohana Reddy, Narayanan Tharangattu Narayanan, Jaime Taha-Tijerina, Juan Peng, Guanhui Gao, Jun Lou, Robert Vajtai, and Pulickel M. Ajayan**

Two-dimensional (2D) atomic layers derived from bulk layered materials are very interesting from both scientific and application viewpoints, as evidenced from the story of graphene. Atomic layers of several such materials such as hexagonal boron nitride (h-BN) and dichalcogenides are examples that complement graphene. The observed unconventional properties of graphene has triggered interest in doping the hexagonal honeycomb lattice of graphene with atoms such as boron (B) and nitrogen (N) to obtain new layered structures. Individual atomic layers containing B, C, and N of various compositions conform to several stable phases in the three-component phase diagram of B–C–N. Additionally, stacking layers built from C and BN allows for the engineering of new van-der-Waals stacked materials with novel properties. In this paper, the synthesis, characterization, and properties of atomically thin layers, containing B, C, and N, as well as vertically assembled graphene/h-BN stacks are reviewed. The electrical, mechanical, and optical properties of graphene, h-BN, and their hybrid structure are also discussed along with the applications of such materials.

1. Introduction

It is well known that dimensionality is one of the most defining parameter for materials, and two dimensional (2D) layered materials are of particular interest from both scientific and application points of views due to their unique planar structures and properties.[1,2] Due to their exceptional structural, physical, and chemical properties, 2D materials are expected to have significant impact on various applications, ranging from electronics to opto-electronics, sensors, catalysis, energy storage, gas separation, and protective coatings. Recent studies have demonstrated that monolayer graphite (so-called graphene (G)), a one-atom-thick planar sheet of sp^2-bonded carbon atoms densely packed in a honeycomb crystal lattice, can exist as a stable material, and it has distinct properties that are not observed in 0D, 1D, or 3D forms of carbon.[3–10] In 2004, Geim and co-workers were successful in isolating single-layer graphite on an insulating substrate (SiO_2) by using a micromechanical cleavage method.[7] After the experimental isolation was realized, scientists have revealed a rich variety of physical phenomenon in this 2D atomic carbon monolayer. For examples, an anomalous quantum Hall effect was reported in graphene, which also serves as direct experimental evidence for the electrons in graphene behaving as massless Dirac fermions, confirming theoretical predictions.[11–14] Graphene shows remarkably high electron mobility at room temperature, and is also characterized as a semi-metal or zero-gap semiconductor with unique electronic properties.[15–17] Further, the fascinating thermal and mechanical properties of graphene make it an attractive candidate for electromechanical resonators, stretchable and elastic matrices for flexible electronic circuitry, ultracapacitors, stable field emitters, and as fillers for electrically conducting flexible nanocomposites.

Prompted by the blossoming research in graphene, people started to explore and isolate other layered materials—such as nitrides, sulfides, selenides, tellurides, and oxides—as 2D atomic sheets.[1,2,18–20] Earlier theoretical and experimental work have shown that unprecedented physical properties were also possible in most of the layered materials by reducing the thickness of their 3D crystal counterparts,[15,16] such as in hexagonal boron nitride (*h*-BN) which is starting to become another fascinating material in this area. An important compound family of the III-V group, the members of the BN family include amorphous BN (a-BN), hexagonal BN (h-BN), cubic BN (c-BN), and the relatively rare wurtzite BN (w-BN). Among them h-BN is the only member to possess a layered structure, with the boron and nitrogen atoms arranged in an sp^2-honeycomb lattice, similar to that of graphene but with complementary properties.[17,21]

Prof. L. Song,[+] Dr. Z. Liu, Dr. A. L. M. Reddy, Dr. N. T. Narayanan, J. Taha-Tijerina, Dr. J. Peng,[++] Dr. G. Gao, Prof. J. Lou, Prof. R. Vajtai, Prof. P. M. Ajayan
Department of Mechanical Engineering & Materials Science,
Rice University, Houston
Texas 77005, USA
E-mail: ajayan@rice.edu
[+] Current address: Research Center for Exotic Nanocarbons, Shinshu University, 4-17-1Wakasato, Nagano 380-8553, Japan
[++] Current address: Key Laboratory of Energy Sources and Chemical Engineering, School of Chemistry and Chemical Engineering, Ningxia University, Yinchuan 750021, P. R. China

DOI: 10.1002/adma.201201792

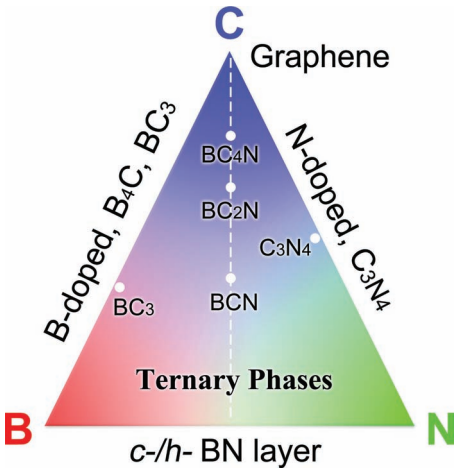

Figure 1. Phase segregation in BCN ternary phase diagram. In this diagram, layered architectures could be built from graphene (C), h-BN (BN), doped graphene (BC and CN), and BCN composite. The C–B and C–N binary chemical compound are possibly formed with certain stoichiometry, such as BC_3, B_2C, and CN_3, while BCN, BC_2N, and BC_4N are located in the ternary phase diagram (dashed line). All these stoichiometries have specific electronic structure and properties.

Unlike graphene, h-BN is an insulator, with a bandgap larger than 5 eV. The bandgap of single-layered h-BN could be up to ~6 eV.[22,23] Many of its properties make it a good candidate to form heterostructures with graphene for device applications.[24,25] Although a series of h-BN based nanostructures have been fabricated, such as h-BN nanotubes,[26–28] nanomesh[21,29,30] and nanoribbon,[31] reports on atomic layers of h-BN are limited due to challenges in their synthesis processes.[17,32,33]

Combining carbon (C) with boron (B) and nitrogen (N) atoms could offer different (B–C–N) layered configurations,[34] as illustrated in **Figure 1**. In addition to the planar (B–C–N)-layer-based materials one could also envision vertical (G/h-BN)-based superlattices. For the former, the phase diagram of B–C–N is rich in the large number of layered hexagonal phase compositions because B, C, and N can substitute with each other and form various new structures due to their similar atomic parameters. Starting with graphene, B substitution can form p-type graphene, while N doping can form n-type graphene. It is also possible to form C–B and C–N binary chemical compounds with different stoichiometry, such as BC_3, BC_2N, and C_3N_4. Early theoretical studies have anticipated that the electronic structure (and bandgap) of $B_xC_yN_z$ will depend on the composition and atomic arrangement of B, C, and N elements in the lattice.[35–38] Figure 1 indicates the possibility of synthesizing p-type and n-type semiconducting graphene by substituting C atoms with B and N atoms, respectively.[39–41] Most interestingly, there are several layered phases in the B–C–N ternary system,[26,35–38,42–46] (such as BCN, BC_2N, BC_4N, BC_3, and C_3N_4), which can be used for a range of applications due to their tunable bandgaps.[47] Similarities in the crystalline structures of graphite and h-BN also point to the possibilities of transforming them to their cubic analogues, diamond and cubic-BN. Ternary solids of these elements with either superhard cubic structures or layered hexagonal structures can be prepared by different

Pulickel Ajayan received his Ph.D. in materials science and engineering from Northwestern University in 1989. After post-doctoral work at NEC Corporation (Japan), he worked as a research scientist at the Laboratoire de Physique des Solides, Orsay (France) and as a Humboldt fellow at the Max-Planck-Institut für Metallforschung, Stuttgart (Germany). In 1997, he joined the materials science and engineering faculty at Rensselaer Polytechnic Institute as an assistant professor. Currently he is the Benjamin M. and Mary Greenwood Anderson Professor in Engineering at Rice University. His research interests are focused on the functional nanostructured materials for a variety of applications.

Li Song received his PhD in Condensed Matter Physics from Institute of Physics, Chinese Academy of Sciences (2006, advisor SiShen Xie). After one and a half years as a Humboldt fellow at LMU Mu.nchen in Germany, he spent three years as a postdoctoral researcher at Rice University. In 2011, he became an associate professor at Shinshu University in Japan. He was promoted to professor at the University of Science and Technology of China by the Thousand Talents Program in 2012. His research interests include the engineering and applications of carbon nanomaterials, 2D layered structures, and multifunctional nanodevices.

Zheng Liu was born in Hubei, China in 1983. He received his B.Sc. (2005) and Ph. D (2010) in Physics from the National Center for Nanoscience and Technology (NCNST), China, under the guidance of Prof. Lianfeng Sun. He is currently a joint postdoctoral fellow at Rice University where he working with Prof. P. M. Ajayan and Jun Lou. His research focuses on the synthesis, characterization, and performance of low-dimensional crystals, including graphene, hexagonal boron nitride, molybdenum disulfide, and their hybridized architectures, as well as carbon nanotubes and metal nanowires.

growth techniques and varied growth parameters.[45,48–55] Some of these structures have complementary electronic structure compared to graphene, doped graphene, and h-BN. It has been theoretically demonstrated that the chemical and physical properties may significantly differ for various B–C–N compositions and arrangements, thus opening up the possibility of tuning electronic properties of these materials. However, it is still challenging to create well-defined B–C–N phases experimentally. Poorly grown h-BCN hybrid films have been obtained using various methods such as thermal chemical vapor deposition (CVD) and plasma-enhanced CVD (PECVD) by thermally decomposing B-, C-, and N-containing precursors.[56–58] However, these as-prepared h-BCN films show very poor crystallization and lack the properties of theoretically predicted h-BCN films. We have recently showed the growth of 2D atomically hybridized layer consisting of random graphene and h-BN domains by a catalytic CVD technique.[59] Reliable method for controlled growth of atomic layers of B–C–N structures will play a key role in understanding the largely unexplored (B–C–N)-rich phase diagram and exploring the properties of various phases.

Graphene/h-BN heterostructure configurations constitute another class of interesting configurations of B–C–N ternary system shown in **Figure 2**. 2D h-BN is found to be an unique layered material building block for producing artificially stacked van der Waals structures such as G/h-BN (Figure 2, right top). h-BN layers have very low lattice mismatch with graphene (~1.8%),[60] have extremely smooth surfaces,[61] and electronically have a wide bandgap. Recent studies indicate that, h-BN atomic layers would be excellent dielectric layers to complement graphene electronics due to its atomically smooth surface (~1/5 roughness of SiO_2)[61] with minimum dangling bonds and charge traps.[62–64] It is further supported by the local spectroscopy measurements that demonstrate that the electron–hole charge fluctuations are reduced by two orders of magnitude as compared with those on silicon oxide.[60] h-BN/G/h-BN layers have also been fabricated for electronic devices with cut-off frequency up to 33GHz.[61] Further calculations indicate a tunable and sizable bandgap (up to 0.34 eV) could be realized by aligning graphene and h-BN in various ways.[65] Most recently, a G/h-BN/G/h-BN/G superlattice field-effect tunneling transistor was fabricated with a high On/Off ratio (50 versus 5, the typical value for pristine graphene).[66]

In this review, we will discuss the recent progresses on 2D atomic layers containing B, C, and N. In particular, the controllable synthesis, characterizations, and applications of graphene and h-BN atomically layered architectures will be presented briefly, including in-plane G/h-BN hybridization, vertically stacked G/h-BN layers, and artificially stacked G/h-BN solids. Such studies are imperative as 2D atomic layers will have high potential for various applications and will inspire new fundamental investigations that could reveal their distinct properties from their bulk counterparts.

2. Atomic Layers Containing Carbon: Graphene

Mechanical exfoliation was the first method employed for preparing single-layer graphene from natural graphite samples or highly oriented pyrolytic graphite (HOPG), which provided graphene flakes with extremely high quality but limited lateral sizes.[7] Liquid exfoliation is the alternative chemical approach to make graphene layers. Weak interlayer van der Waals forces in these crystals can be easily overcome by ultrasound waves produced in low-surface-tension liquids. The majority of papers have described the synthesis of graphene-like sheets, which are chemically functionalized with species such as hydroxyls and epoxides, by dispersion and exfoliation of graphene oxide (GO). However, the chemical modification of graphene sheets disrupts the electronic properties due to significant number of defects introduced during treatments. Recently, large-scale synthesis of defect-free graphene sheets have been achieved by exfoliating graphite in organic solvents such as *N*-methyl-pyrrolidone.[67] Currently, this liquid exfoliation method has been extended to the synthesis of atomic layers from a variety of layered solids such as MoS_2, WS_2, $MoSe_2$, $MoTe_2$, $TaSe_2$, $NbSe_2$, $NiTe_2$, BN, and Bi_2Te_3.[68] Epitaxial growth method as well as chemical vapor deposition methods have also been used to produce graphene layers from silicon carbide or metal substrate such as Cu and Ni foils, respectively.[69–73] The possibility of large-scale electronics based on SiC-epitaxial graphene layers has been reported.[74–76] On the other hand, the CVD method is considered as a facile way for growing graphene via simple thermal decomposition of hydrocarbons on the metallic surface or via surface segregation of carbon.[41,77–86] A variety of transition metals (Ni, Cu, and Co) and a vast number of different carbon sources from gaseous (CH_4, C_2H_2), liquid (*n*-hexane), and solid (poly(methyl methacrylate) (PMMA)) carbon-containing precursors have been tried for the synthesis of graphene. The typical growth temperature for CVD is ~800–1100 °C. It is found that the carbon solubility in the metal

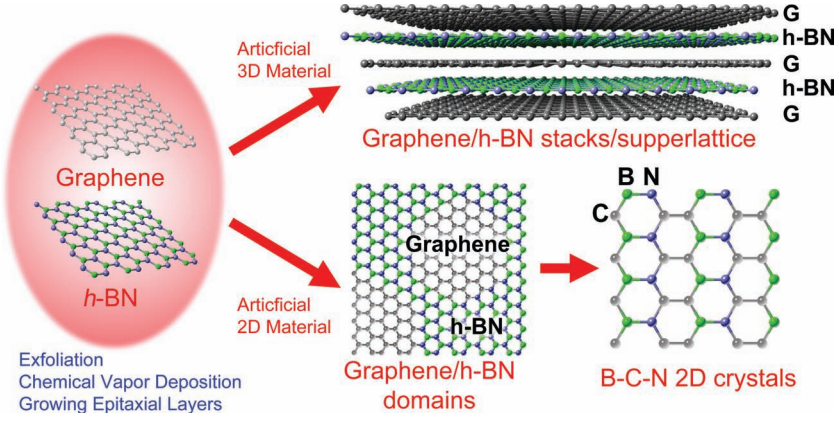

Figure 2. Schematics of possible approaches for artificial B–N–C layers. Exfoliation, chemical vapor deposition, and epitaxial growth are three common methods to synthesize carbon- and BN-based atomic layered structures such as graphene and h-BN. The B–N–C layers could be constructed vertically for G/h-BN stacks/superlattice, or in-plane for G/h-BN domains and finally B–C–N 2D crystals with a controllable stoichiometry.

and the growth conditions determine the deposition mechanism which ultimately also defines the morphology and thickness of the graphene films. For examples, the number of layers of graphene formed could be controlled well, from a single layer to few layers.[79] The highest electron mobility for as-transferred films has been reported to be more than 30 000 $cm^2/(V\ s)$ on h-BN substrate, but in most cases the mobility values range from ~700–3000 $cm^2/(V\ s)$[41,81,83,87] due to various defects.[88–90] For example, grain boundaries in polycrystalline graphene are believed to be an obstacle to electron transport. However, careful refinements in growth techniques have pushed the limits to obtain supersized single-crystal domains.[83,88,91] Currently, the lateral size of graphene layers grown by CVD can be scaled up to 30 inches with a sheet resistance of few hundreds Ω/□.[84] In our group we have successfully grown single, bi- and few graphene layers on copper foils and stainless steel by using *n*-hexane solvent as carbon source in a CVD system.[92–95]

Due to the absence of a substantial bandgap, the on/off ratio of graphene field effect transistors is typically around 5, which is one hindrance to its use in future electronics.[65] Several ways could open the bandgap in graphene, including doping graphene with foreign elements such as nitrogen,[41,95,96] engineering of graphene to a nanoribbons[6,39,97,98] or quantum dots,[99–102] and by designing hybridized graphene with other layered materials such as h-BN and MoS_2.[66,103]

2.1. Synthesis, Characterization, and Properties of Graphene and Graphene Nanostructures

Large-scale, high-quality monolayer graphene can be grown on Cu foils by CVD method as shown in **Figure 3**. The size of the CVD-grown graphene (Figure 3a) can be large depending on the size of the Cu foils. The graphene films are continuous and uniform as characterized in the optical image (Figure 3b). The Raman spectrum of single-layer graphene is shown in the inset of Figure 3b. The D peak is nearly invisible, which suggests good quality graphene films; other characteristics include the intensity ratio of 2D/G in Raman spectra up to 4.2 and the full-width at half maximum (FWHM) of the 2D peak of ~24 cm^{-1}. These values are comparable to mechanically exfoliated monolayer graphene. The number of layers could be well controlled from monolayer to a few layers. High-resolution TEM (HRTEM) examination confirms that the films have one, two, three, or four layers depending on growth conditions (Figure 3c). The typical sheet resistance of as-grown graphene film is ~2–10 kΩ/□.

The graphene could be grown on various substrates such as Cu/Ni/stainless foils, Cu/Ni nanowires, nanoporous Ni, Ni foams, Cu/Ni spheres, and some other alloys, enabling several unique graphene-based architectures. The graphene nanostructures can also be made by other approaches, such as by cutting metal nanoparticles (Figure 3d) and by liquid exfoliation.[104] Cutting graphene layers can be done via catalytic hydrogenation and the etched structures show preferred crystallographic orientations for the edges. This unique approach makes it possible to obtain graphene pieces of various shapes with the same edge type and sharp edges, for example triangles, and this could impact applications such as shape-enhanced magnetism

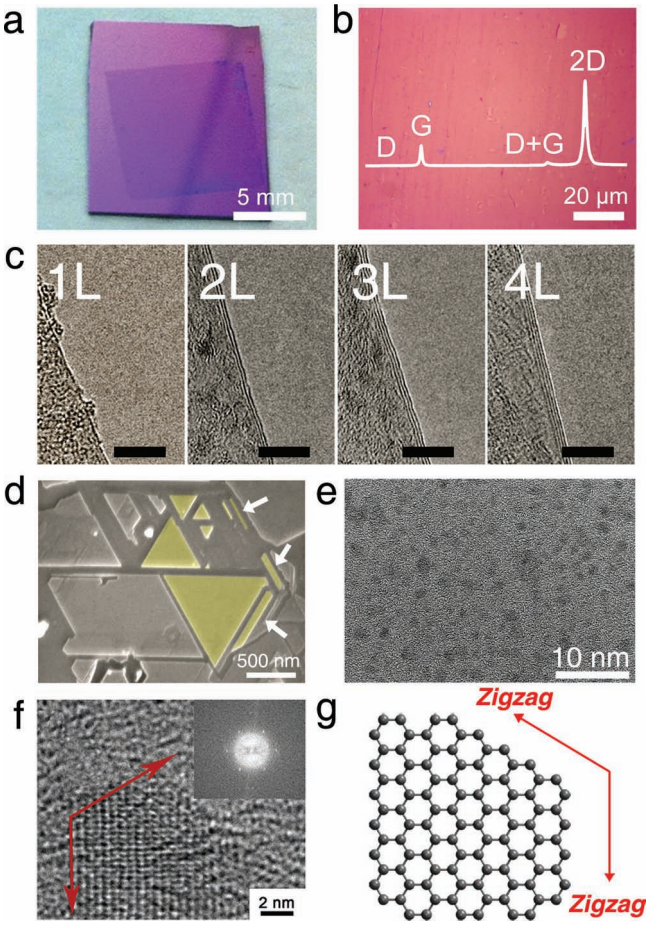

Figure 3. Synthesis and characterizations of graphene and graphene nanostructures. a) Photograph of CVD graphene on 285 nm SiO_2. Size: ~1 cm × 1 cm. b) Optical image of high-quality CVD graphene covering SiO_2, uniformly and continually. Inset: Raman spectrum of monolayered graphene. c) TEM images of CVD-grown graphene showing 1–4 layers (1L–4L, respectively). All scale bars are 5 nm. d) Graphene structures cut by Ni nanoparticles. The white arrows mark some nanoribbons. e) TEM and f) HRTEM images of GQDs derived from carbon fibers. g) Schematic of the zigzag edge of GQDs. Reprodued with permission.[92,101,104] Copyright 2010 and 2012 American Chemistry Society.

in graphene materials. Work is in progress in several groups to obtain graphene structures that have controlled shapes and edge structures.

Graphene quantum dots (GQDs) constitute another graphene nanostructure with fascinating optical and electronic properties.[99,100,102,105–109] We have demonstrated a wet chemically derived GQDs from acidic treatment of carbon fibers (CF). The results reveals that these GQDs show very low cytotoxicity and excellent biocompatibility, which can be used as an eco-friendly material for bioimaging.[101] Figure 3e shows a typical TEM image of GQDs synthesized by chemical exfoliation and cutting of micrometer-sized pitch-based carbon fibers (CF). It was found that the fiber derived GQDs exhibit a relatively narrow size distribution between 1 and 4 nm with high crystallinity and most of them are terminated with zigzag edges (Figure 3e–g). The UV–visible absorption spectra of GQDs

reveal a clear blue shift from 330 to 270 nm with the reaction temperature increasing from 80 to 120 °C. The GQDs synthesized at varying temperatures show blue, green, or yellow emission colors under UV light. The emission spectra reveal the distribution of emission wavelength of the as-synthesized GQDs and can be tailored by varying the size of the GQDs by changing process parameters. We chose the green GQDs to perform the cellular imaging because cell's nucleus was stained with 4′,6-diamidino-2-phenylindole (DAPI), which shows blue color under imaging. Our work demonstrated that GQDs can be prepared in a scalable manner starting from commercial carbon fibers and used in high-contrast bio-imaging and other applications such as opto-electronics.

The high charge-carrier mobility in graphene has resulted in strong interest in graphene-based high-speed electronic devices. Various graphene-based terahertz sources and detectors have been proposed as the frequency of plasma waves, the bandgap of graphene nanoribbons,[110,111] and the tunable bandgap in bilayer graphene lies in the terahertz range.[97,112–120] The channel potential distribution in a graphene field-effect transistor (FET) has been imaged by scanning photocurrent imaging technique,[121] which has also revealed potential gradients occurring at monolayer–multilayer graphene interfaces.[122] Our collaborators in Germany have studied time-resolved picosecond photocurrents in freely suspended graphene contacted by metal electrodes.[123] They introduced a pump-probe photocurrent spectroscopy to graphene-based devices to resolve their photo-electric response up to 1 THz.[124] In experiments, it was demonstrated that terahertz radiation was generated in optically pumped graphene. In their work, spatially resolved picosecond photocurrents were measured in freely suspended graphene contacted by metal strip-lines. It was shown that both built-in electric fields and the photothermoelectric effect contribute to the photocurrent generation at graphene–metal interfaces. In addition, optical pumping of the freely suspended graphene gave rise to strong photocurrent oscillations that originate from terahertz radiation emitted from an electron–hole plasma in the optically pumped graphene.[123]

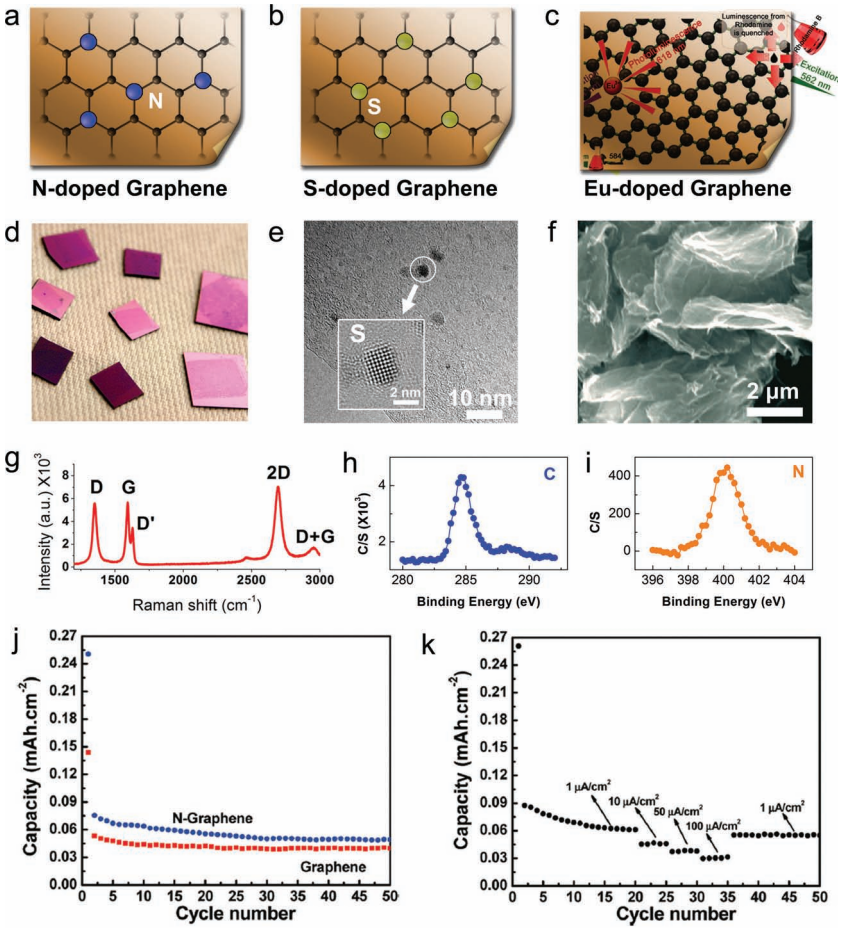

Figure 4. Graphene doping and its application in Li-ion batteries. a,b) Schematics of N- and S-doped graphene. c) Schematic illustration of Eu-doped graphene and its photoluminescence effect. d) Photographs of S-/N-doped graphene. e) TEM image of S-doped graphene grown by mixing sulfur powder with (*n*-hexane) as the liquid carbon source. Sulfur superlattice (black regions) is found to be imbedded in the graphene matrix. A typical sulfur region is shown in the inset. f) SEM image of Eu-doped graphene. g) Typical Raman spectrum of S-/N-doped graphene. The prominent D and D′ peaks come from the sample defects which are believed to be the results of doping, as compared to the Raman spectrum of pristine graphene shown in the inset of Figure 3b. h,i) XPS spectra of C and N peaks in N-doped graphene. j) Variation in discharge capacity versus cycle number for the pristine graphene and N-doped graphene cycled at a rate of 5 μA/cm^2 between 3.2 and 0.02 V vs Li/Li$^+$ in 1 M solution of $LiPF_6$ in 1:1 (volume ratio) mixture of ethylene carbonate (EC) and dimethyl carbonate (DMC) as the electrolyte. k) Rate capability studies of N-doped graphene films: Discharge capacity versus cycle number at various current rates. Reproduced with permission.[94,95,140] Copyright 2010 American Chemistry Society and 2011 Wiley-VCH Verlag Gmbh & Co. KGaA.

2.2. Substitutional Doping of Graphene

Pristine graphene is a zero-bandgap semiconductor, and subsequently limiting its applications in electronics and other applications. Doping graphene lattice substitutionally with guest atoms such as nitrogen,[85,95,125–132] sulfur,[125,133] boron,[134] and fluorine[135–137] (**Figure 4**a,b) opens up the bandgap of graphene and changes its chemical and surface characteristics. In some cases (e.g., boron), the dopants remain in the sp^2 hybridized configuration, but in some cases (e.g., fluorine) sp^3 bonding can be introduced, and the latter can change the planar nature of graphene. Several approaches can be exploited for doping graphene. Growing graphene using a carbon source that contains or mixed with precursors having doping elements is one approach; materials such as PMMA, dimethylacetamide (DMAc), or *n*-hexane, can be used as carbon sources.[85] We have also mixed carbon sources such as *n*-hexane with dopants

such as DMAc for N-doped graphene and with dimethyl sulfoxide (DMSO) for S-doped graphene. Another approach is annealing graphene layers with doping agents such as gaseous NH_3.[126] Yet another approach is the interaction and functionalization of graphene with metals such as Li, Xe, and Eu.[138–140] We have synthesized Eu-doped graphene using reduced graphene oxide as a starting material via a solution chemistry approach (Figure 4c). Figure 4d shows optical images of S- and N-doped graphene. Figure 4e is a representative TEM image of S-doped graphene. The sulfur superlattice embedded in the graphene matrix is shown in the inset. Figure 4g–i show the typical Raman spectrum and X-ray photoelectron spectroscopy (XPS) spectra of N-doped graphene. The D and D′ peaks in the Raman spectrum become prominent due to the doping effect, and this in conjunction with other techniques such as XPS and TEM were used to understand the bonding configurations of the dopants in the graphene lattice. Figure 4f shows a typical scanning electron microscopy (SEM) image of Eu-doped graphene showing luminescence due to the presence of Eu. Such a doping strategy offers a new paradigm in the engineering of graphene analogues for tuning optical and electronic properties.[140]

2.3. Graphene and Doped Graphene for Energy Storage

Recent studies have established graphene as a promising anode material for Li-ion batteries, supercapacitors, fuel cells, solar cells, etc.. Atomically thin nature and high surface area of the graphene electrodes grown directly on current collector substrates are of special interest in developing high-power thin-film lithium ion batteries. We have explored Li-ion battery and supercapacitor applications for one- to a few-layer pristine and doped graphene.[141,142] Graphene and nitrogen-doped graphene layers that are directly grown on current collector substrates (Cu and stainless steel) showed enhanced Li-ion storage capacity and excellent rate capabilities.

Galvanostatic charge/discharge measurement were conducted at a constant current of 10 μA cm^{-2} between 3.2 and 0.02 V by constructing a Li half-cell using few-layered graphene and nitrogen doped graphene electrodes as the working electrodes and Li foil as the counter and reference electrode.[95] Figure 4j and k indicate that the reversible discharge capacity of N-doped graphene increases when compared to that of pristine graphene, which can be attributed to the topological defects present in the N-doped graphene electrode which act as additional sites for Li-ion storage. N-doped graphene electrodes have been further tested at different current rates, even at very high current rates of operation, such as 100 μA/cm^2, excellent capacity retention of 60% of the nominal capacity was observed (Figure 4k). The results of high-rate electrochemical studies prove that the N-doped graphene electrode could be used as a very good high rate Li-ion battery electrode. The direct contact between the active materials (N-doped graphene) and the current collector (Cu foil) leads to reduced electrical resistance, hence, resulting in a high electrode rate capability. Direct growth of graphene or doped graphene on current collector substrates makes this a feasible process to be integrated into the current thin-film battery manufacture technology. We have also demonstrated a novel concept of in-plane supercapacitor using graphene mono/few-layer electrodes.[141] Typically, graphitic carbon-based materials are randomly oriented with respect to the current collector in a conventional stacked geometry in supercapacitors. In such cases, the electrolyte ions are often limited from penetrating far inside the graphitic planes. This lowers the complete utilization of the electrochemical surface area of graphene layers and consequently limits the extent of the electrochemical double layer formed at the interface. In devices such as thin-film supercapacitors, modification in the architecture can be made to tune performances and graphene may play an important role in such design concepts.

3. Atomic Layers Containing Boron and Nitride: Hexagonal BN (h-BN)

Hexagonal boron nitride (so called white graphite due to its structural similarity to graphite) comprises alternating boron and nitrogen atoms in a 2D honeycomb lattice. Within each layer of h-BN, boron and nitrogen atoms are bound by strong covalent bonds, whereas the layers are held together by weak van der Waals forces. Therefore, monolayer h-BN is structurally similar to graphene, and individual BN layers could be isolated from bulk h-BN crystals.[2,18,143] Similar to graphene, few-layered h-BN can be synthesized via CVD, liquid exfoliation, and traditional mechanical exfoliation methods. Due to its wide bandgap, h-BN is a good insulator. So it can serve as a complementary material and substrate to graphene to build high-mobility graphene devices. The strong BN bond makes an h-BN atomic layer a mechanically strong material, quite analogous to graphene. Furthermore, due to its electrical insulation and high thermal conductivity, layered h-BN could be utilized as a filler material in many engineering fluids and composites.

3.1. Synthesis and Characterization of h-BN

The h-BN atomic layers can also be obtained on Cu/Ni foil by CVD at ~1000 °C with ammonia borane or borazine source as a precursor. In contrast to the synthesis of graphene where monolayers can be easily grown over large area, methods for preparing uniform single h-BN atomic layers is still a challenge.[17,32,33,144,145] Several groups around the world are working on this, and these efforts will certainly bring new opportunities to exploit unique properties and potential applications of 2D h-BN layers. Recently, our group showed that uniform and continuous h-BN layers could be successfully grown using a thermal catalytic CVD method.[23] In our experiment, copper foil (Cu) and nickel (Ni) were used as a catalytic substrate, and ammonia borane (NH_3-BH_3) was used as the starting precursor (more detail can be seen in Refs. [23] and [146]). **Figure 5**a shows typical h-BN films grown on Cu foil and then transferred onto silica substrate. The SEM image of as-grown h-BN layers shown in Figure 5b reveals that the film is quite uniform and continuous except for some wrinkles that were introduced during the transfer process. The white arrow indicates a region where h-BN is peeled off, exposing the SiO_2 substrate. TEM observations showed that the thicknesses of h-BN

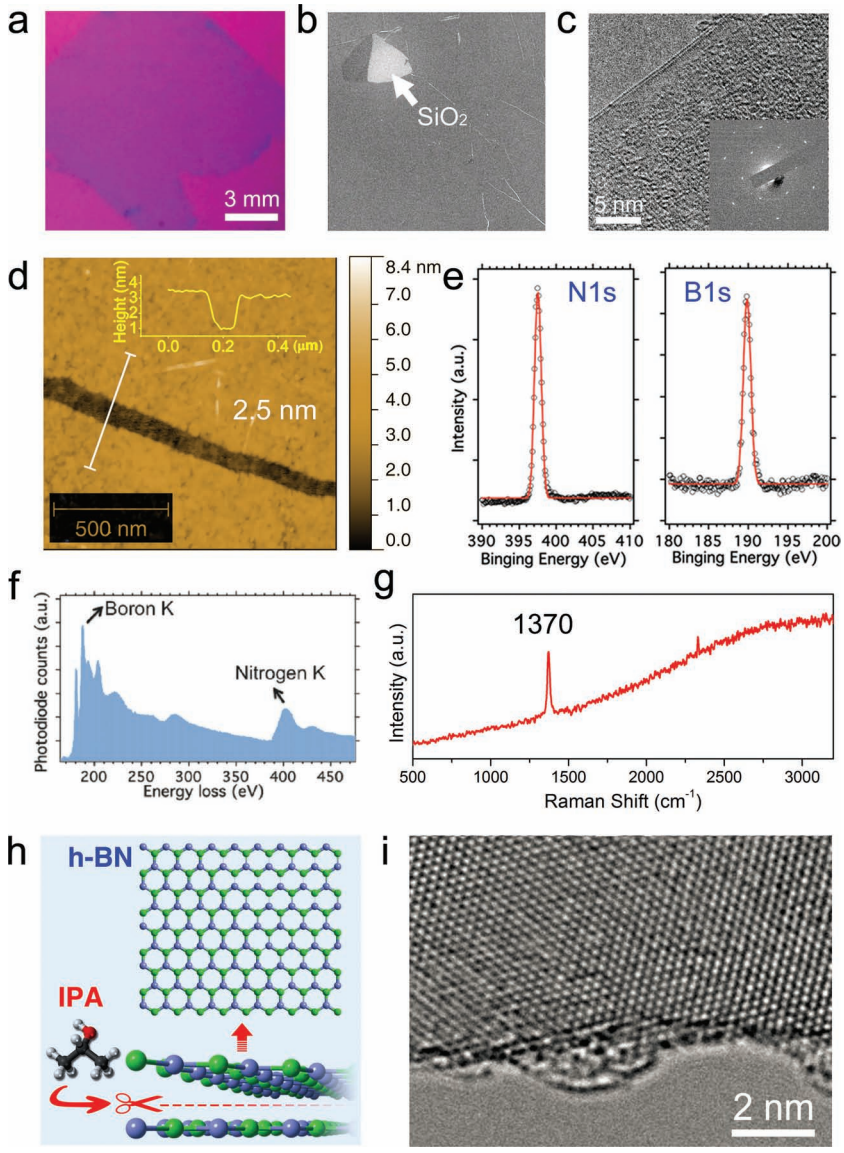

Figure 5. Synthesis and characterizations of h-BN atomic layers. a) Photograph of few-layered h-BN on SiO_2 synthesized via the CVD method. Size: ~12 mm × 12 mm. b) SEM image shows continuous and uniform h-BN film. The light grey region is SiO_2, marked by the white arrow. c) TEM image of a typical h-BN film with two layers. Inset: selected area electron diffraction (SAED) patterns showing six-fold-symmetry. d) An AFM topography image of few-layered h-BN. The grey stripe is SiO_2 and the rest is an h-BN atomic layer with a thickness of ~2.5 nm. e) XPS spectrum of B and N 1s core level, located at ~190 and 398 eV. f) EELS spectrum showing the K edges of boron and nitrogen. g) Raman spectrum of an h-BN film using an excitation wavelength of 514.5 nm. The signal-to-noise ratio for few-layered h-BN is much lower than that of bulk h-BN. h) Schematic illustration of 2D h-BN nanosheets fabricated using the liquid exfoliation method. i) HRTEM image of a typical h-BN nanosheet from a liquid exfoliated flake with ~5 atomic layers. Partially reproduced with permission.[23,143,146] Copyright 2010 and 2012 American Chemistry Society.

films are around 1 nm, mainly consisting of two to three layers (Figure 5c). The electron diffraction pattern in the inset of Figure 5c clearly indicates the hexagonal structure of h-BN films of high quality.[28,147–149] We have further studied the topography of h-BN layers by atomic force microscopy (AFM) (Figure 5d). The thickness of the h-BN film is ~1–3 nm measured from the line profile of the AFM topography image as indicated in the insert of Figure 5d. The XPS spectra of as-grown h-BN layers (Figure 5e) show the B 1s-core level at 189.9 eV and the N 1s-core level at 397.6 eV, which is very close to that in bulk h-BN.[150,151] Both the B 1s and the N 1s spectra indicate that the bonding for B and N atoms is through the direct B—N bonding (in contrast to B–C or C–N), implying that the hexagonal phase exists in the CVD-grown materials as h-BN layers. Figure 5f is a typical electron energy loss spectroscopy (EELS) sepctrum, clearly showing the K-edge of boron and nitrogen as the arrows indicate. Figure 5g shows typical Raman spectra that were taken from the h-BN layers. The E_{2g} vibrating mode of h-BN atomic layers is found to be at ~1370 cm^{-1}. The B-N vibrational peak for h-BN few-layers up-shifts to higher frequencies compared with that for the bulk h-BN perhaps due to stresses introduced in these atomically thin layers.[27,152,153] Finally, Figure 5h shows schematic illustration of individual h-BN layers peeled off from bulk h-BN lattice by liquid exfoliation technique, another important method to prepare 2D h-BN materials. The HRTEM image is shown in Figure 5i. According to the electron diffraction patterns, we observed that the crystallinity of exfoliated h-BN layers and the rotational disorder associated with the individual layers in the stacking.

3.2. Properties of h-BN

Previous investigations have shown that bulk h-BN is a wide bandgap material. The UV–visible absorption spectrum was used to investigate the optical energy bandgap of our CVD-grown h-BN films based on its optically induced transitions. Large h-BN films were first transferred onto an optical quartz plate, and the quartz background was subtracted using a blank quartz plate as the reference substrate. The nanometer-thick h-BN film is highly transparent and can transmit over 99% of the light within a spectrum range of 200–900 nm. A typical absorption spectrum is shown in **Figure 6**a. The absorption spectrum displays one sharp absorption peak at 203 nm. Based on Tauc's formulation,[152] the calculated bandgap wavelength is about 223 nm, which corresponds to an optical bandgap of 5.56 eV. Previous theoretical calculations of band structures for a single layer of h-BN anticipated that equivalent bands did not cross each other and a 6 eV bandgap was predicted,[22] which is in good agreement with our UV–visible absorption results. Considering two to five

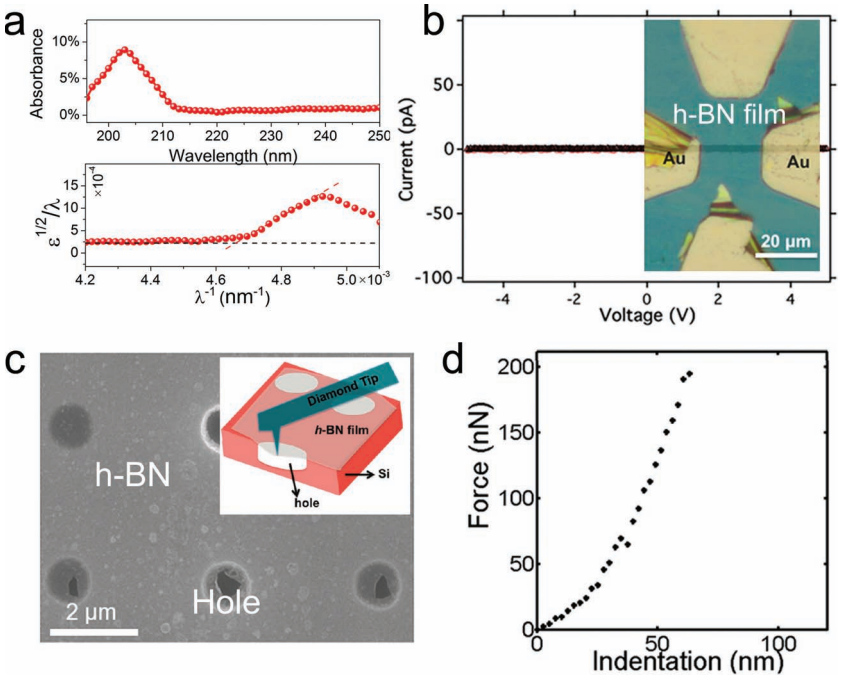

Figure 6. Optical, electrical, and mechanical properties of CVD-grown h-BN atomic layers. a) UV–vis spectra of few-layered h-BN. Top panel shows the plot of absorption versus wavelength, and bottom panel is the plot of $\varepsilon^{1/2}/\lambda$ versus $1/\lambda$. Here ε is the optical absorbance and λ is the wavelength. The optical bandgap is estimated to be ~5.6 eV via the linear fitting in the bottom panel. b) Current–voltage characteristic of h-BN films, indicating h-BN is a good insulator. Inset is the device fabricated by photolithography. c) SEM image of a large h-BN film spanning an array of circular holes with 1 μm diameter. Inset is a schematic illustration of the AFM-assisted nanoindentation experiments performed on a suspended h-BN membrane. d) Measured representative force versus displacement curve. Reproduced with permission.[23] Copyright 2010 American Chemistry Society.

layers of our h-BN films, the measured bandgap is expected to be smaller than the theoretically calculated bandgap for a single layer as the layer–layer interaction increases the dispersion of the electronic bands and tends to reduce the bandgap.[22] However, it is larger than that of bulk h-BN (5.2–5.4 eV).[22,154] We performed electrical measurements on devices based on h-BN films, fabricated by standard lithography technique (Figure 6b inset: the optical image of the h-BN device) and found that the h-BN films are very good insulators.

Earlier studies have demonstrated the unique mechanical properties of 2D atomic layers.[98–103,105] The bending stiffness of the monolayer graphene is critical in attaining the structural stability for both suspended and supported graphene sheets, which in turn could have an impact on the electronic properties. The in-plane mechanical properties (elastic modulus and strength) of monolayer graphene have been deduced from experiments.[106–109] Measurements conducted on few-layer graphene yielded spring constants of 1 to 5 N m^{-1}. A Young's modulus of 0.5 TPa was extracted and a breaking strength was found to be 42 N m^{-1} suggesting graphene as a promising material for mechanical resonator applications.[110–112]

We also studied the mechanical properties of CVD-grown h-BN atomic layers using AFM-assisted nanoindentation measurements.[23] h-BN films were first transferred onto a pre-patterned holey substrate. The transferred membranes were observed to be freestanding over many circular wells, as shown in Figure 6c. The mechanical properties of the suspended h-BN films were probed by indenting the center of each free-standing membrane using a diamond tip. The mechanical properties of were calculated using equations reported in the literature for similar configurations.[155] A representative force versus displacement curve is shown in Figure 6d. The obtained values of the elastic constant range from 220 to 510 N m^{-1} for the h-BN films with thicknesses of 1–2 nm. The measured 2D modulus of h-BN in our case is lower than the theoretically predicted values (270 N m^{-1} for a single BN layer).[155,156] This could be caused by the layer distribution of stacking faults in the CVD-grown films,[157] or errors in estimating the exact diameter of the holes and the boundary condition of the membrane in contact with the substrate. The breaking strength of h-BN films was measured by loading the membranes to the breaking point. A typical fracture test curve suggested that the film broke at deflections of about 70 nm and forces of about 221 nN. A continuum model was used to determine the maximum stress of a clamped circular membrane[155] and the calculated breaking strength was found to be ~8.8 N m^{-1} for ~1 nm thick h-BN film. The lower breaking stress we obtained for the h-BN film compared with monolayer graphene could be due to possible defects in our freestanding as-grown membranes.[156,157] Somewhat reduced stiffness of the h-BN layers can be due to either compliance at the edges (hole perimeter), or due to presence of defects. Possible defects distribution in the films could also contribute to the relatively lower values in our AFM-assisted nanoindentation experiments. In summary, it can be seen that the mechanical properties of h-BN layers are in the same range as that of graphene, suggesting that h-BN atomic layers could feature an ideal structure to support graphene-based electronics and devices, in addition to its own interesting properties and applications.

3.3. Exfoliated h-BN for Thermal Management

Development of nanomaterials for energy management is another thrust area of our present research. 2D layered-material-based nanofluids can be developed, and they can either be used to reduce energy loss due to friction and wear in mechanical parts or to dissipate energy from high-power thermal or electrical systems.[158] One pioneering research in this area is to use 2D layer materials as nanofillers in heat transfer fluids.[159–165] As an insulating material with very high thermal conductivity, h-BN layers surpass other nanofillers and are an attractive material for high thermal conductivity and electrically insulating composites. Recently, we have studied the synthesis

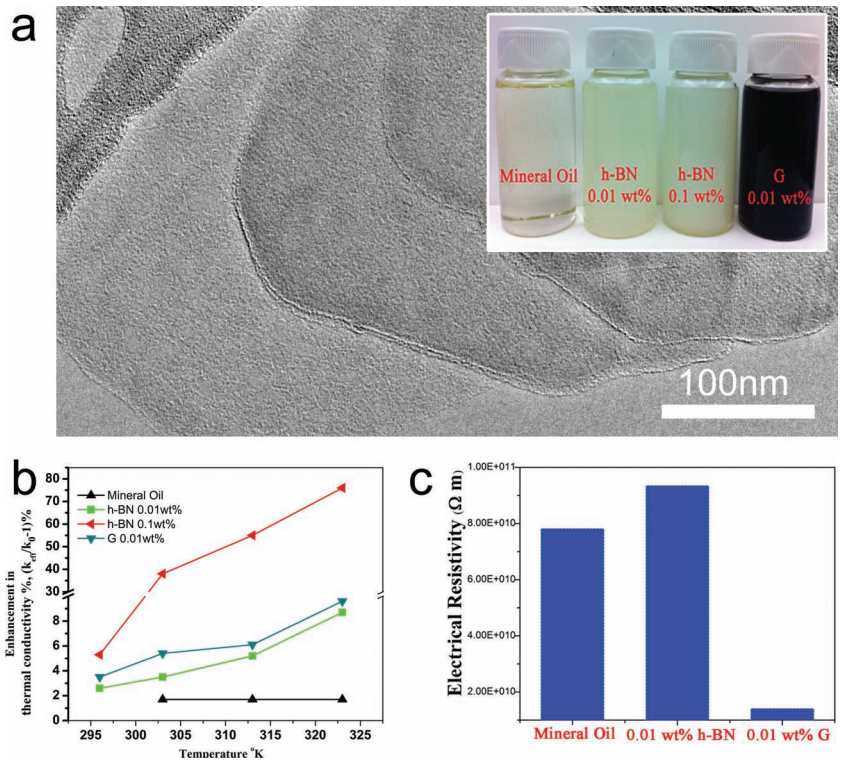

Figure 7. Electrically insulating thermal nanofluids containing few-layered h-BN fillers. a) Typical TEM image of h-BN few-layered flakes prepared by liquid exfoliation. Inset is optical image of liquids of pristine MO, MO/h-BN, and MO/G showing different colors. b) Temperature-dependent effective thermal conductivity enhancement of various nanofluids. c) Electrical resistivity variation of the nanofluids. Reproduced with permission.[143] Copyright 2012 American Chemistry Society.

and characterization of novel nanofluids containing exfoliated h-BN and graphene layers in mineral oils (MO).[143]

The TEM image of exfoliated few-layered h-BN flakes are shown in **Figure 7**a. Inset is the optical image of pure MO, MO/0.01% h-BN, MO/0.1% h-BN and MO/0.01% graphene (wt%) liquid. Figure 7b shows the enhancement in thermal conductivity with the increase in weight fraction of h-BN or graphene and increase in measurement temperatures. For instance, 0.1%wt addition of h-BN in MO shows an enhanced thermal conductivity of around 76%. This large enhancement in thermal conductivity even with low fractions of nanomaterials is made possible by the large surface area provided by the exfoliated layers. The variations of thermal conductivity were measured at 323 K for different h-BN/MO fluids with varying h-BN concentration. The thermal conductivity of h-BN/MO fluids is found to have gradually increased with h-BN filler concentration. h-BN/MO fluids exhibited an enhancement in thermal conductivity with increase in both temperature and filler fraction, indicating Brownian motion and percolation mechanism are contributing to the thermal conductivity. The h-BN/MO exhibits the lowest dissipation factor (DF), while graphene/MO possesses an enhanced value compared to MO at all measured temperatures. Since DF represents the ratio of equivalent series resistance (ESR) to capacitive reactance, the decrease in DF indicates the decrease in dielectric losses in the material. The electrical resistivity of the nanofluids is also found to be affected by various nanofillers (Figure 7c). The h-BN/MO exhibited higher resistivity, while graphene/MO showed lower resistivity compared to pristine MO. To further understand the stability of the nanofluids, shear viscosity studies were also conducted. Temperature-dependent shear viscosity data for different concentrations of h-BN/MO indicates that h-BN/MO nanofluids are relatively stable colloidal systems. It was found that the pour point, which is the lowest temperature at which the fluid can flow (pumpable temperature), seems to be affected by the nanofillers of h-BN and graphene. The lowering of the pour point can be attributed to the nanoscale dimensions of the fillers (here h-BN) and high intermolecular interactions and liquid layering (MO) with the h-BN.[166,167] The results also indicate that the stable Newtonian nanofluid with 2D fillers of h-BN in MO is electrically insulating fluid and has a lower freezing point than that of pure MO. These unique h-BN/MO nanofluids may be the next-generation thermal nano-oils for various energy management systems. The conducting graphene nanofluids can be utilized for static energy dissipation in oil tanks and other systems, where the nanofiller needs to be conducting and at the same time low filler loadings are desired to produce higher electrical conductivity. Our recent studies also show that they can easily form stable suspensions in water. These results suggest that these nanofluids with exfoliated atomic layers containing carbon, boron, and nitrogen atoms can be very promising candidates for various types of energy and thermal management platforms.

4. Atomic Layers Containing B, C, and N: Hybrid Hexagonal BCN (h-BCN)

Earlier theoretical studies predicted that inorganic BCN layer-based nanostructures could be formed, and such predictions were confirmed almost immediately, thereby initiating the emergence of the field of BCN materials.[26,34–40,42–46,56–59,168,169] There have been experimental demonstrations of doping B and N in carbon systems, including BCN-based nanotubes[170–173] and BCN-based nanostructures,[174–176] although fully homogenized BCN phases of controlled compositions have not been experimentally reported.[26,39,40,43,168] In almost all experimental studies, it has been observed that there is a strong tendency in these systems to form segregated C and BN domains making the formation of true alloy phases difficult.

4.1. Synthesis and Characterization of h-BCN Atomic Layers

Our group has recently reported a systematic route to synthesize 2D hexagonal BCN hybrid structures consisting of a patchwork

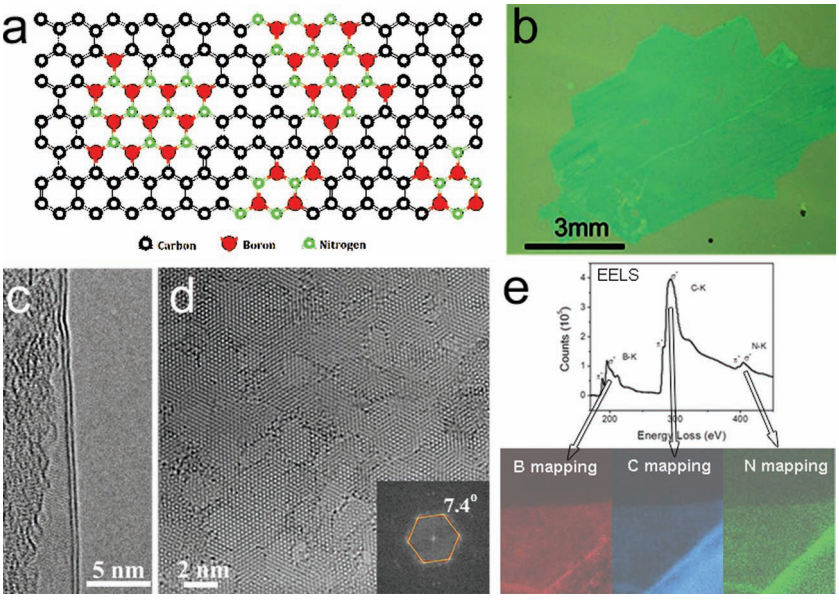

Figure 8. Synthesis and characterizations of h-BCN atomic layers. a) Atomic model of hybrid h-BCN layer consisting of hybridized h-BN and graphene domains. b) Optical microscopy image of hybrid h-BCN film. c) High-resolution and d) atomistic TEM images of two hybrid h-BCN layers. The inset in (d) is the FFT patterns of the two-layer region. e) EELS spectra taken from as-grown samples showing K-shell excitations of B, N, and C. The bottom GIF (energy filtered imaging technique) images show uniform elemental distribution of B, C, and N. Reproduced with permission.[59] Copyright 2010 Nature Publishing Group.

of h-BN and C nanodomains (illustrated in **Figure 8**a).[59] To synthesize h-BCN, methane and ammonia borane were introduced at the same time to act as precursors for carbon and BN, respectively. The atomic ratio of B, C, and N can be tuned by controlling the experimental parameters, although the B/N ratio remains almost always close to unity, suggesting a strong tendency for the formation of BN composition. Figure 8b shows an optical microscopy image of hybrid h-BCN film transferred onto a silicon substrate, revealing that the film is quite uniform over large area.

High-resolution TEM observations in Figure 8c indicate these h-BCN films are about 1 nm thick, consisting of mainly 2–3 layers. The typical atomic structure of h-BCN film was shown in Figure 8d. The inset is the fast Fourier transform (FFT) from the image revealing two sets of hexagonal spots with a very small rotational angle about 7.4°, indicating that the film mainly consists of double layers with a hexagonal atomic arrangement in the lattice. Different Moiré patterns can be also seen in Figure 8d due to the lack of AB stacking registry between the two graphene layers.[177] Most of our TEM observations reveal that the majority of the multilayer structures of as-grown h-BCN films are inturbostratic stacking, and only a very small area show well graphitized AB Bernal stacking. The EELS results shown in Figure 8e shows three visible edges starting at 185, 276, and 393 eV, corresponding to the characteristic K-shell ionization edges of B, C, and N, respectively.[150,151] The EELS edge structure proves that all three elements are sp^2 hybridized, indicating that the atomic films grown on Cu possess a hexagonal structure consisting of B, C, and N. The inset GIF (energy filtered imaging technique) images in Figure 8e reveal that all three elements are uniformly distributed in the detected area. However, it has been a challenge to resolve the individual h-BN domains and graphene domains which overlap in projection from the multiple layers of BCN present in the films.

The UV–visible absorption spectrum was carried out for investigating optical energy bandgap of the h-BCN film. Compared to pristine graphene and h-BN atomic layers, h-BCN films show high transparency at long wavelengths with two absorption peaks. The absorption edges have been studied in h-BCN with 65 at.% C.[22,178] The optical bandgap was estimated to be of 4.48 eV, which comes from the h-BN domains in the film. However, it is smaller than that of pure h-BN sample, indicating the effect of C doping on BN domains. We found that increasing C content to 85 at.% lowers this values to 3.85 eV. The optical bands of 1.62 and 1.51 eV were obtained from the samples with 65 and 85 at.% C, respectively. This absorption edge is thought to be from h-BN-doped graphene domains.[59]

It has been anticipated that the electronic structure and properties of B–C–N will be quite different depending on the composition and atomic arrangement of B, C, and N elements in the lattice.[35,36,38] We have investigated the electrical properties of the CVD-grown h-BCN films.[59] **Figure 9**a shows a typical h-BCN based device connected to four electrodes. It is found that the electrical conductivity of h-BCN increases with increasing percentage of carbon (Figure 9b). The pure h-BN is an insulator, while the BCN ribbon with 94% carbon has a very low resistivity of around 10^{-3} Ω cm. Our results suggest that we can easily control the electrical properties of the h-BCN films from insulating to highly conducting by tuning the carbon concentration. Figure 9c shows the back-gate-dependent electrical response of h-BCN ribbons (40 at% C) at room temperature. The h-BCN field-effect transistor exhibits ambipolar semiconducting behavior, and the results indicate that the h-BCN films have an atomic structure consisting of hybridized h-BN and graphene domains, since theoretical and experimental investigations have indicated that B–C–N mixed phases are typically p-type semiconductors. We want to point out here that the above electrical transport data do not support C/BN stacked structure; otherwise, the conductivity should be dominated by the highly conducting graphene layer. Figure 9d shows typical temperature dependence of the resistance for a pristine graphene sample and h-BCN ribbon with 90 at% carbon in zero magnetic field. As is clearly seen, the resistance increases monotonically as the temperature decreases, which indicates that pristine graphene acts as a semiconductor with zero bandgap in agreement with previous reports. In contrast to pristine graphene, h-BCN shows a clear insulator-to-metal transition with a peak at around 10 K, where a negative derivative of the resistance as a function of temperature (dR/dT) corresponds to insulating behavior, and the positive sign is empirically associated with

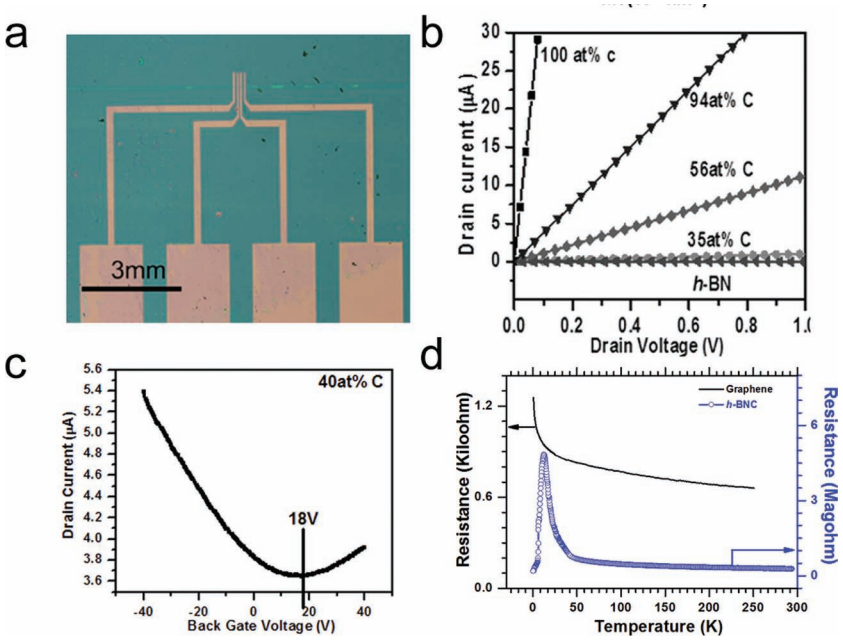

Figure 9. Electrical properties of h-BCN atomic layers. a) Optical image of h-BCN-ribbon-based FET device with four electrodes. b) Electrical properties of h-BCN with different carbon percentages tested at room temperature. c)The drain current as a function of the back gate voltage for an FET device based on a h-BCN ribbon (with 40 at.% carbon). The drain source voltage is fixed at 1 V. d) Temperature dependence of the resistance for pristine graphene and h-BCN ribbon with 90 at.% carbon, demonstrating an interesting insulator-to-metal transition in the h-BCN atomic layer. Reproduced with permission.[59,181] Copyright 2010 Nature Publishing Group.

metallic behavior. Experimentally, on the insulating side of the transition, the two terminal resistance of h-BCN monotonically increases to reach a maximum as the temperature decreases from room temperature to around 10 K. On the metallic side of the transition, the resistance drops drastically by more than one order of magnitude as the temperature decreases from 10 K to the lowest achieved value of 500 mK. As discussed above, the h-BCN samples consist of a percolating graphene network embedded within h-BN domains. Since the BN domains have a very large bandgap (~5 eV) acting like an "infinite" barrier, the electronic and transport properties of the graphene network will be similar to those of the graphene nanohole superlattices.[179] Small bandgaps can be opened in graphene as a result of quantum confinement and/or spin-polarization at a specific C–BN boundary.[30,179,180] We suggest that the observed insulator-to-metal transition in h-BCN is the result of the coexistence between two distinct mechanisms, namely, percolation through metallic graphene networks and hopping conduction between edge states on randomly distributed insulating h-BN domains. Such h-BCN structures and phases provide a unique opportunity to study disordered 2D systems and the ability to tune electronic properties with and without the presence of a magnetic field.

4.2. Direct Deposition of h-BN on Graphene

There is a strong interest to create stacks of graphene and h-BN layers for electronic applications, and this has been achieved by transferring the respective layers produced by mechanical exfoliation.[64] Interesting devices can be built from the stacking of graphene and h-BN atomic layers, for example a capacitor (G/h-BN/G) with the thinnest dielectric layer possible. These devices are being investigated by several groups around the world. However, a facile and scalable synthesis approach to make G and h-BN stacked structures could enable a lot of fascinating research in this area. Recently, it has been reported that the on/off ratio of graphene devices could reach 50 by vertically and alternatively stacking graphene and h-BN atomic layers.[66] Our group has demonstrated the direct CVD growth of G and h-BN stacks via a two-step process,[146] which could pave the way for scale-up synthesis of G/h-BN stacks over large areas.

The stacked G/h-BN structure consists of alternatively stacked graphene and h-BN atomic layers, as illustrated in **Figure 10**a. Figure 10b shows an optical image of as-grown G/h-BN stacked structure transferred on a silica substrate. In the optical microscopy image, the striped area is graphene region, and the rest of the area is G/h-BN. Some exposed SiO_2 regions in light purple can also be seen. Figure 10c shows a SEM image of G/h-BN stacks. The left region is pure graphene and the right one is G/h-BN stack. Figure 10d shows the TEM morphology of the G/h-BN stacked film. The inset of d is the corresponding diffraction patterns consisting of two groups of six-fold symmetry spots, indicating a possible G/h-BN stacked structure. High-resolution TEM in Figure 10e reveals that the stacked structure consists of two to few layers. Figure 10f is the TEM image corresponding to the zero energy loss maps, and Figure 10g–i are elemental mapping showing the elemental distribution of carbon, nitrogen, and boron.

Raman spectra with 514.5 nm laser excitation was done on the G/BN stacked films and compared with that from pure graphene layers. Figure 10j shows that the G and 2D peaks of pure graphene are located at 1597 and 2695 cm^{-1}, and the intensity of the 2D peak is much higher than that of the G peak. The disorder-induced Raman D-peak at 1350 cm^{-1} is quite small, indicating the high quality of the graphene. For the pure h-BN, a strong peak at 1369 cm^{-1} is observed which is ascribed to the E_{2g} model of B–N vibration.[22,152,178] The spectrum of the G/BN stacked film is shown in Figure 10k, in which four peaks are seen at 1356, 1595, 1622, and 2710 cm^{-1}. Here, the peak at 1356 cm^{-1} can be from the B–N vibration and D mode of graphene with the rest of the peaks coming from pure graphene layers. These results are distinct from our previous report on hybridized boron nitride and graphene domains (h-BCN) and pristine h-BN. In the work of h-BCN films, it was found that the Raman peaks were induced by hybridized graphene and h-BN domains together, showing up as a mixed broad D band at 1360 cm^{-1} and a mixed suppressed 2D band at 2700 cm^{-1}.

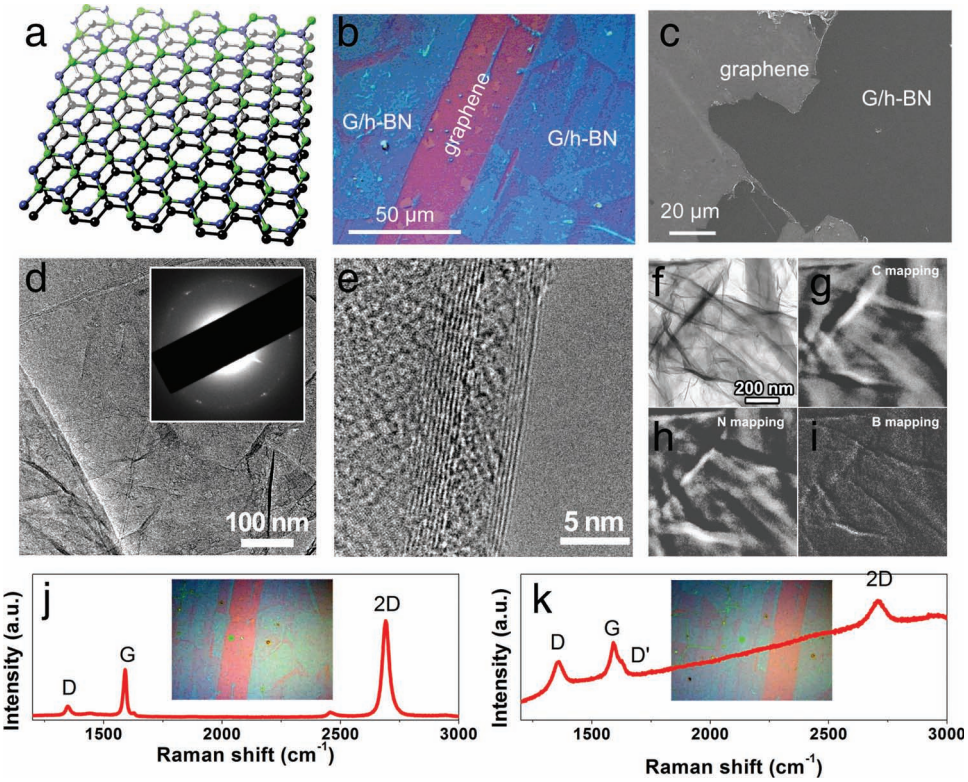

Figure 10. Synthesis and characterizations of graphene/h-BN stacks. a) Atomic model of a graphene and h-BN stack. b) Optical microscopy image of graphene/h-BN stacked atomic layers supported by the SiO_2 substrate. The wide-stripe is graphene, located at the center. Some tiny SiO_2 regions are noted. The rest of the area is covered by G/h-BN stacked layers. c) SEM image of G/h-BN landscape. The right region is pure graphene while the rest is G/h-BN stack in dark black. d) TEM images of G/h-BN stacked atomic layers showing its top morphology. Inset is the corresponding diffraction patterns. e) TEM image of edges of G/h-BN atomic layers showing a few-layered graphene and h-BN. f-i) TEM images of original G/h-BN atomic layers (f) and the GIF mapping of C (g), N (h), and B (i), showing an uniform distribution for all elements. j,k) Raman spectra obtained from pure graphene and G/h-BN stacked film, with 514 nm excitation laser. The insets correspond to optical images of the regions where Raman data were collected from. Reproduced with permission.[146] Copyright 2011 American Chemistry Society.

For the G/h-BN stacked structure, its Raman peaks originate from the vibration modes corresponding to h-BN and graphene independently. Therefore, one can clearly see the photoluminescence in the whole spectrum background induced by the top h-BN layers and the intrinsic characteristic G and 2D peaks originating from the bottom graphene layers. The Raman mappings clearly suggest the uniform and continuous coverage of graphene and h-BN atomic layers grown on the surface of the copper foil.

The XPS spectra from the stacked G/h-BN structure are presented in **Figure 11**a and a depth profile test was used to confirm the stacked layer structure. A high-energy argon ion-beam was used to sputter the film layer by layer from its top surface, and the spectra were analyzed (Figure 11a) for B, N, and C. The analysis showed that the B and N core level peaks correspond to those from h-BN, and the C peak corresponds to graphene, once again proving the stacked geometry.[150,151] Figure 11b is a schematic illustration of how the argon ion-beam sputters G/h-BN layers sequentially. The atomic concentration and intensity decrease for both B and N as Ar ion etching continues, suggesting h-BN as the top layer being removed from the as-grown stacks during sputtering. Figure 11c shows the evolution of atomic concentration and intensity for elements B, N, and C. In addition, also we have demonstrated that h-BN we grew h-BN using HOPG as a substrate. This h-BN film is found to be extremely uniform and continuous; no defects or holes that would expose the HOPG underneath are observed.

4.3. Direct Growth of Graphene on h-BN

Compared to the direct growth of h-BN on graphene, the reverse growth of graphene on h-BN was demonstrated via a general transfer-free method. The growth was demonstrated for large areas of uniform bilayer graphene on h-BN and other insulating substrates, from solid carbon sources such as films of poly(2-phenylpropyl)methysiloxane (PPMS), PMMA, polystyrene (PS), and poly(acrylonitrile-*co*-butadiene-*co*-styrene) (ABS).[93] The carbon feedstock were deposited on the insulating substrates and then capped with a layer of nickel. At 1000 °C, under low pressure and a reducing atmosphere, the carbon source could be transformed into a bilayer graphene film on the insulating substrates. The Ni layer was then removed by dissolution, making

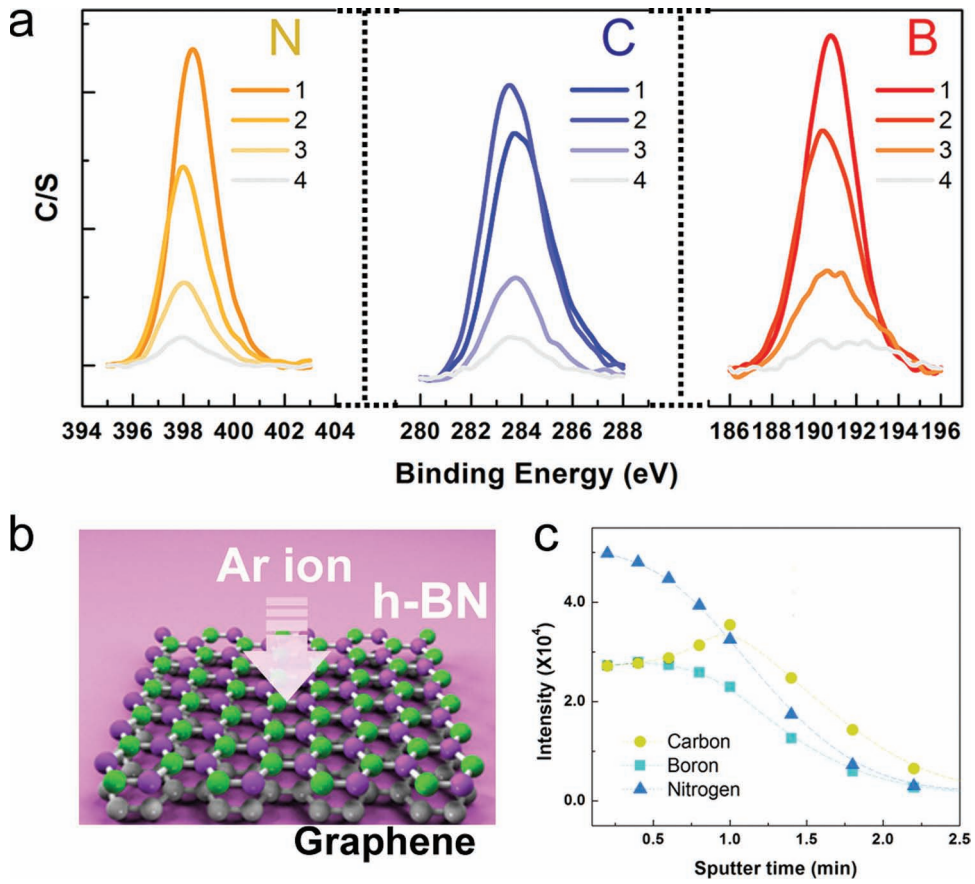

Figure 11. Determine the stacking order of graphene and h-BN layers by XPS depth-profiling. a) Evolution of count/second for B, N, and C 1s core levels during alternative etching of Argon ion. It indicates that the signal from B and N become weaker during etching (from 1 to 4), while the strongest signal from C is obtained after etching for 1 min. b) Schematic illustration of how the argon ion-beam sputters G/h-BN layers. c) The relative atomic concentration with increasing etching time. Reproduced with permission.[146] Copyright: 2011 American Chemistry Society.

it possible for the bilayer graphene to directly sit on the insulator such as h-BN with no traces of polymer left from a typical transfer step. More details of the growth process were described the literature.[146] The sheet resistances of the graphene films on the h-BN substrates were found to be ~2000 Ω/□.

4.4. Artificially Stacked G-BN van-der-Waals Solids

For large-scale synthesis of atomic layers, liquid exfoliation has been generally employed. Solids containing G and h-BN randomly stacked together can be obtained by taking the exfoliated layers and mixing them together. The chemical exfoliation of bulk h-BN and graphite powders in organic solvents with sonication and centrifugation allows good dispersion of individual layers. The approach of mixing exfoliated atomic layers of various compositions to obtain randomly layer stacked solids is new and could lead to enormous possibilities of new types of van der Waals stacked materials.

We have demonstrated the above concept with layers of graphene and h-BN. The h-BN dispersion in isopropanol solvent was first prepared and then mixed with graphene dispersions. The G/h-BN hybrid dispersion was found to be stable and remain dispersed even after several months. These dispersions when filtered produce films that contain layers of both graphene and h-BN. The overall composition of these solids can be controlled by varying the initial concentration of the mixture. **Figure 12**b shows a typical TEM image of the chemically exfoliated and artificially stacked solids consisting of randomly stacked layers of graphene and h-BN. EELS spectra in Figure 12a and c identify the atomic composition of the G/h-BN hybrid; K-shell ionization edges of B, C, and N are visible at 189, 289, and 407eV, respectively. They indicate that isolated graphene and h-BN layers have been alternately stacked together to form a random artificial structure bound by van der Waals force. The chemical exfoliation approach could be used to create artificial materials, made from the van der Waals stacking of robust atomic layers of different layered solids with vastly different properties. Figure 12d–f show Raman spectra and mappings that have been used to study the distributions and possible stacking orders of these hybrid solids.

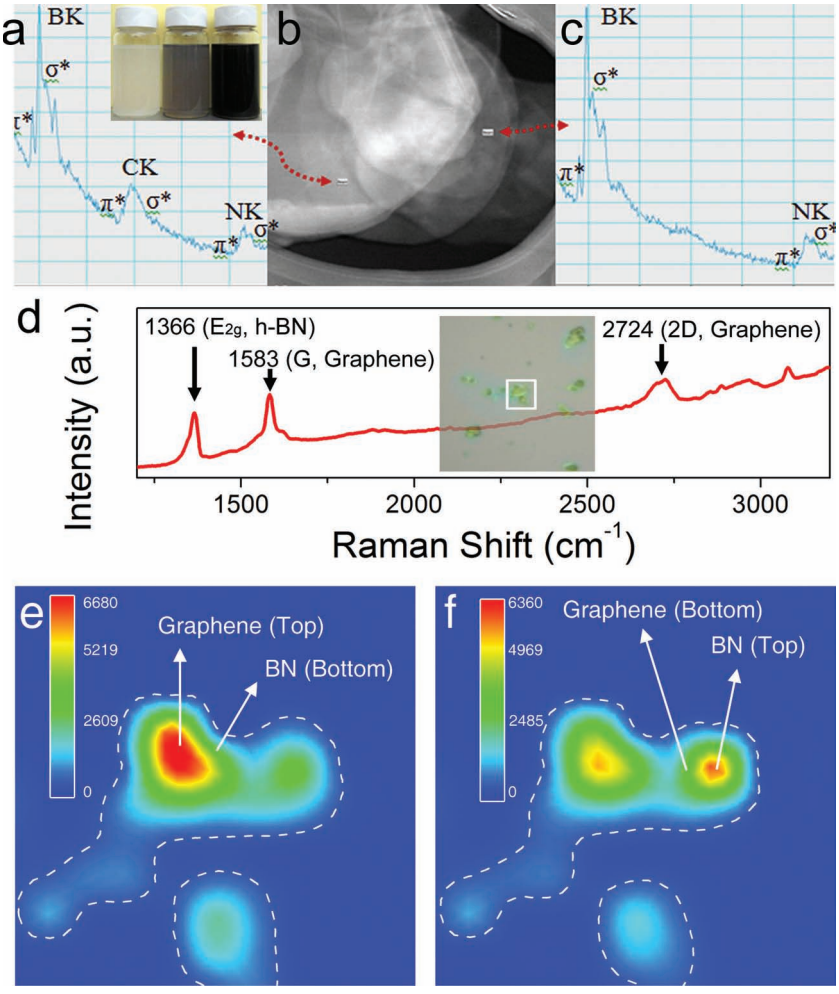

Figure 12. Synthesis and characterizations of graphene/h-BN artificial solid. a-c) TEM image and elemental analysis of G/h-BN artificial stacks prepared by the chemical exfoliation method. b) TEM image of G/h-BN stacks. a,c) Corresponding EELS spectra from the regions marked in (b). Inset in a: Dispersions of h-BN (isopropanol, IPA), graphene (dimethylformamide, DMF) and hybrid of h-BN and graphene. d) Typical Raman spectrum of G/h-BN stacks. The peak located at ~1366 cm^{-1} is from the E_{2g} vibration of h-BN. This asymmetry peak indicates a possible D peak from graphene. Peaks located at ~1583 and 2724 cm^{-1} are the G and 2D peaks of graphene, respectively. Inset: optical image for G/h-BN solid where the Raman spectrum is collected. e,f) Raman mappings of the region marked in a white square in the inset of (d) at a Raman shift of 1580 (e) and 1370 (f) cm^{-1}. Reproduced with permission.[182] Copyright 2012 American Chemical Society.

5. Conclusion and Future Outlook

In this article, we have briefly reviewed the recent progress of our group at Rice University on the synthesis, characterization, property measurements, and applications of 2D atomic layers containing B, C, and N. The BCN phase diagram is rich with various to-be explored phases with properties ranging from metallic to semiconducting to insulating. Two major phases that have received tremendous attention recently are graphene (pure C) and h-BN. These have been isolated or grown as uniform atomic layers, and related properties are unveiled to a large degree. There are still possibilities for creating hybrid structures with these components because graphene and h-BN are structurally similar. Since they are meanwhile electrically dissimilar, various interesting devices could arise from the controlled engineering of these phases, both in two dimensions as well as in three-dimensional stacking.

BCN nanostructures were theoretically expected to show a rich variety of physical properties and to enable numerous possible technological applications in the fields of nano-electronics, optical devices, field emission, catalysis, lubrication, and gas storage. Much effort from the experimental side as mentioned before have been performed to synthesize BCN-based nanostructures with various geometries. The hunt for 2D BCN atomic layers beyond graphene and h-BN has recently started. However, the research of B/C/N systems is still very much in its early stages. Many challenges related to the controllable synthesis and detailed characterizations need to be addressed before a comprehensive exploration of the under-explored regions of the BCN phase diagram. These challenges include how to prepare atomic layer phases with controlled compositions, how to determine the location of various atoms using techniques such as scanning tunneling microscope (STM) and scanning tunneling spectroscopy (STS), and how to correlate experimental results on electronic and magnetic properties to the determined structure and theoretical predictions.

The synthesis of several BCN layered phases (e.g., BCN, BC_2N, BC_3) could follow recent successes in the synthesis of graphene and h-BN over metal substrates using CVD or other techniques. The methods used for co-doing B and N into nanocarbons could be another possible way for realizing uniform BCN layers. Several theoretical predictions exist showing the wide range of properties of the BCN phases, and it is for the experimentalists to explore this phase diagram and attempt to synthesize atomic layers of different compositions of B, N, and C. In addition to the full-fledged phases with specific compositions, there also exists interest in doping graphene with B and N with small amounts. The same holds for doping of h-BN with carbon. These doped structures should exhibit interesting electronic properties. The trick is, as we have shown in the review, to keep the dopants well distributed in the lattice of graphene or h-BN as they have strong tendencies to segregate and form domains of pure carbon and BN. Experimentalists will have to find the right processing windows via systematic trial and error to pin down novel BCN phases as well as uniformly doped graphene and BN lattices, and this will be no small challenge. While new applications of well-known phases such as graphene and h-BN keep emerging, we believe that the search for BCN

layered structures will have a far reaching impact on the area of 2D atomic layers.

Acknowledgements

Financial support came from the Army Research Office through the MURI program on novel free-Standing 2D crystalline materials focusing on atomic layers of nitrides, oxides, and sulfides and the Office of Naval Research (ONR) through the MURI program on graphene. L.S. acknowledges the Exotic Nanocarbons, Japan Regional Innovation Strategy Program by Excellence JST in Japan, the Recruitment Program of Global Experts, and the CAS Hundred Talent Program in China. A.L.M.R. acknowledges the support from Army Research Office. T.N.N and P.M.A acknowledge funding sponsorsed by the DOD: Air Force Office of Scientific Research for the Project MURI Award No. FA9550-12-1-0035. J.L. acknowledges the support by the Welch Foundation grant C-1716. We thank Akshay Mathkar, Alexander W. Holleitner, Bipin Kumar Gupta, Charudatta Galande, Gang Shi, Hao Lu, Hemtej Gullapalli, Hui Gao, Jiangnan Zhang, Jiaqi Huang, Kaushik Balakrishnan, Ken Hackenberg, Leo Prechtel, Lijie Ci, Lulu Ma, Mingjie Wang, Neelam Singh, Rebeca Romero, Sanketh Gowda, Xiaobo Zhan, and Yongji Gong for their assistance and for helpful discussions.

Received: May 3, 2012
Published online: July 13, 2012

[1] C. Lee, Q. Li, W. Kalb, X.-Z. Liu, H. Berger, R. W. Carpick, J. Hone, *Science* **2010**, *328*, 76.
[2] K. S. Novoselov, D. Jiang, F. Schedin, T. J. Booth, V. V. Khotkevich, S. V. Morozov, A. K. Geim, *Proc. Natl. Acad. Sci. USA* **2005**, *102*, 10451.
[3] D. R. Dreyer, R. S. Ruoff, C. W. Bielawski, *Angew. Chem. Int. Ed.* **2010**, *49*, 9336.
[4] R. Mas-Balleste, C. Gomez-Navarro, J. Gomez-Herrero, F. Zamora, *Nanoscale* **2011**, *3*, 20.
[5] H. B. Heersche, P. Jarillo-Herrero, J. B. Oostinga, L. M. K. Vandersypen, A. F. Morpurgo, *Nature* **2007**, *446*, 56.
[6] Y.-W. Son, M. L. Cohen, S. G. Louie, *Nature* **2006**, *444*, 347.
[7] A. H. Castro Neto, F. Guinea, N. M. R. Peres, K. S. Novoselov, A. K. Geim, *Rev. Mod. Phys.* **2009**, *81*, 109.
[8] S. Das Sarma, S. Adam, E. H. Hwang, E. Rossi, *Rev. Mod. Phys.* **2011**, *83*, 407.
[9] R. R. Nair, P. Blake, A. N. Grigorenko, K. S. Novoselov, T. J. Booth, T. Stauber, N. M. R. Peres, A. K. Geim, *Science* **2008**, *320*, 1308.
[10] K. S. Novoselov, A. K. Geim, S. V. Morozov, D. Jiang, Y. Zhang, S. V. Dubonos, I. V. Grigorieva, A. A. Firsov, *Science* **2004**, *306*, 666.
[11] A. K. Geim, K. S. Novoselov, *Nat. Mater.* **2007**, *6*, 183.
[12] M. I. Katsnelson, K. S. Novoselov, A. K. Geim, *Nat. Phys.* **2006**, *2*, 620.
[13] K. S. Novoselov, A. K. Geim, S. V. Morozov, D. Jiang, M. I. Katsnelson, I. V. Grigorieva, S. V. Dubonos, A. A. Firsov, *Nature* **2005**, *438*, 197.
[14] Y. B. Zhang, Y. W. Tan, H. L. Stormer, P. Kim, *Nature* **2005**, *438*, 201.
[15] J. Zhou, Q. Wang, Q. Sun, P. Jena, *Phys. Rev. B* **2010**, *81*.
[16] E. Almahmoud, I. Kornev, L. Bellaiche, *Phys. Rev. B* **2010**, *81*, 064105.
[17] A. Nag, K. Raidongia, K. P. S. S. Hembram, R. Datta, U. V. Waghmare, C. N. R. Rao, *ACS Nano* **2010**, *4*, 1539.
[18] J. N. Coleman, M. Lotya, A. O'Neill, S. D. Bergin, P. J. King, U. Khan, K. Young, A. Gaucher, S. De, R. J. Smith, I. V. Shvets, S. K. Arora, G. Stanton, H. Y. Kim, K. Lee, G. T. Kim, G. S. Duesberg, T. Hallam, J. J. Boland, J. J. Wang, J. F. Donegan, J. C. Grunlan, G. Moriarty, A. Shmeliov, R. J. Nicholls, J. M. Perkins, E. M. Grieveson, K. Theuwissen, D. W. McComb, P. D. Nellist, V. Nicolosi, *Science* **2011**, *331*, 568.
[19] S. Najmaei, Z. Liu, P. M. Ajayan, J. Lou, *Appl. Phys. Lett.* **2012**, *100*, 013106.
[20] Y. Zhan, Z. Liu, S. Najmaei, P. M. Ajayan, J. Lou, *Small* **2012**, *8*, 966.
[21] M. Corso, W. Auwärter, M. Muntwiler, A. Tamai, T. Greber, J. Osterwalder, *Science* **2004**, *303*, 217.
[22] X. Blase, A. Rubio, S. G. Louie, M. L. Cohen, *Phys. Rev. B* **1995**, *51*, 6868.
[23] L. Song, L. Ci, H. Lu, P. B. Sorokin, C. Jin, J. Ni, A. G. Kvashnin, D. G. Kvashnin, J. Lou, B. I. Yakobson, P. M. Ajayan, *Nano Lett.* **2010**, *10*, 3209.
[24] Y. Kubota, K. Watanabe, O. Tsuda, T. Taniguchi, *Science* **2007**, *317*, 932.
[25] K. Watanabe, T. Taniguchi, H. Kanda, *Nat. Mater.* **2004**, *3*, 404.
[26] W.-Q. Han, W. Mickelson, J. Cumings, A. Zettl, *Appl. Phys. Lett.* **2002**, *81*, 1110.
[27] J. Wu, W.-Q. Han, W. Walukiewicz, J. W. Ager, W. Shan, E. E. Haller, A. Zettl, *Nano Lett.* **2004**, *4*, 647.
[28] N. G. Chopra, R. J. Luyken, K. Cherrey, V. H. Crespi, M. L. Cohen, S. G. Louie, A. Zettl, *Science* **1995**, *269*, 966.
[29] A. Goriachko, Y. He, M. Knapp, H. Over, M. Corso, T. Brugger, S. Berner, J. Osterwalder, T. Greber, *Langmuir* **2007**, *23*, 2928.
[30] J. Bai, X. Zhong, S. Jiang, Y. Huang, X. Duan, *Nat. Nanotechnol.* **2010**, *5*, 190.
[31] K. J. Erickson, A. L. Gibb, A. Sinitskii, M. Rousseas, N. Alem, J. M. Tour, A. K. Zettl, *Nano Lett.* **2011**, *11*, 3221.
[32] A. Nagashima, N. Tejima, Y. Gamou, T. Kawai, C. Oshima, *Phys. Rev. Lett.* **1995**, *75*, 3918.
[33] W. Auwarter, H. U. Suter, H. Sachdev, T. Greber, *Chem. Mater.* **2004**, *16*, 343.
[34] A. Rubio, *Nat. Mater.* **2010**, *9*, 379.
[35] A. Rubio, J. L. Corkill, M. L. Cohen, *Phys. Rev. B* **1994**, *49*, 5081.
[36] Y. Miyamoto, A. Rubio, M. L. Cohen, S. G. Louie, *Phys. Rev. B* **1994**, *50*, 4976.
[37] Y. K. Yap, *B-C-N Nanotubes and Related Nanostructures*, Springer, Dordrecht **2009**.
[38] Z. Wengsieh, K. Cherrey, N. G. Chopra, X. Blase, Y. Miyamoto, A. Rubio, M. L. Cohen, S. G. Louie, A. Zettl, R. Gronsky, *Phys. Rev. B* **1995**, *51*, 11229.
[39] T. B. Martins, R. H. Miwa, A. J. R. da Silva, A. Fazzio, *Phys. Rev. Lett.* **2007**, *98*, 196803.
[40] M. Deifallah, P. F. McMillan, F. Cora, *J. Phys. Chem. C* **2008**, *112*, 5447.
[41] D. Wei, Y. Liu, Y. Wang, H. Zhang, L. Huang, G. Yu, *Nano Lett.* **2009**, *9*, 1752.
[42] J. Kouvetakis, T. Sasaki, C. Shen, R. Hagiwara, M. Lerner, K. M. Krishnan, N. Bartlett, *Synthetic. Met.* **1990**, *34*, 1.
[43] D. Golberg, Y. Bando, P. Dorozhkin, Z. C. Dong, *MRS Bull.* **2004**, *29*, 38.
[44] E. Hernández, C. Goze, P. Bernier, A. Rubio, *Phys. Rev. Lett.* **1998**, *80*, 4502.
[45] A. Y. Liu, R. M. Wentzcovitch, M. L. Cohen, *Phys. Rev. B* **1989**, *39*, 1760.
[46] M. O. Watanabe, S. Itoh, T. Sasaki, K. Mizushima, *Phys. Rev. Lett.* **1996**, *77*, 187.
[47] S. Ulrich, T. Theel, J. Schwan, H. Ehrhardt, *Surface Coatings Technol.* **1997**, *97*, 45.
[48] Y. K. Yap, Y. Wada, M. Yamaoka, M. Yoshimura, Y. Mori, T. Sasaki, *Diam. Relat. Mater.* **2001**, *10*, 1137.
[49] A. W. Moore, S. L. Strong, G. L. Doll, M. S. Dresselhaus, I. L. Spain, C. W. Bowers, J. P. Issi, L. Piraux, *J. Appl. Phys.* **1989**, *65*, 5109.

[50] A. R. Badzian, *Mater. Res. Bull.* **1981**, *16*, 1385.
[51] A. Derre, L. Filipozzi, F. Peron, *Journal De Physique. IV: JP* **1993**, *3*, 195.
[52] A. Essafti, E. Ech-chamikh, J. L. G. Fierro, *Diam. Relat. Mater.* **2005**, *14*, 1663.
[53] W. R. L. Lambrecht, B. Segall, *Phys. Rev. B* **1993**, *47*, 9289.
[54] K. Montasser, S. Hattori, S. Morita, *Thin Solid Films* **1984**, *117*, 311.
[55] M. Yamada, M. Nakaishi, K. Sugishima, *J. Electrochem. Soc.* **1990**, *137*, 2242.
[56] M. Kawaguchi, T. Kawashima, T. Nakajima, *Chem. Mater.* **1996**, *8*, 1197.
[57] K. Suenaga, C. Colliex, N. Demoncy, A. Loiseau, H. Pascard, F. Willaime, *Science* **1997**, *278*, 653.
[58] R. B. Kaner, J. Kouvetakis, C. E. Warble, M. L. Sattler, N. Bartlett, *Mater. Res. Bull.* **1987**, *22*, 399.
[59] L. Ci, L. Song, C. Jin, D. Jariwala, D. Wu, Y. Li, A. Srivastava, Z. F. Wang, K. Storr, L. Balicas, F. Liu, P. M. Ajayan, *Nat. Mater.* **2010**, *9*, 430.
[60] J. Xue, J. Sanchez-Yamagishi, D. Bulmash, P. Jacquod, A. Deshpande, K. Watanabe, T. Taniguchi, P. Jarillo-Herrero, B. J. LeRoy, *Nat. Mater.* **2011**, *10*, 282.
[61] W. Han, T. Taychatanapat, A. Hsu, K. Watanabe, T. Taniguchi, P. Jarillo-Herrero, T. Palacios, *Electron Device Letters, IEEE* **2011**, *32*, 1209.
[62] C. Oshima, A. Itoh, E. Rokuta, T. Tanaka, K. Yamashita, T. Sakurai, *Solid State Commun.* **2000**, *116*, 37.
[63] G. Giovannetti, P. A. Khomyakov, G. Brocks, P. J. Kelly, J. van den Brink, *Phys. Rev. B* **2007**, *76*, 073103.
[64] C. R. Dean, A. F. Young, I. Meric, C. Lee, L. Wang, S. Sorgenfrei, K. Watanabe, T. Taniguchi, P. Kim, K. L. Shepard, J. Hone, *Nat. Nanotehcnol.* **2010**, *5*, 722.
[65] R. Quhe, J. Zheng, G. Luo, Q. Liu, R. Qin, J. Zhou, D. Yu, S. Nagase, W.-N. Mei, Z. Gao, J. Lu, *NPG Asia Mater* **2012**, *4*, e6.
[66] L. Britnell, R. V. Gorbachev, R. Jalil, B. D. Belle, F. Schedin, A. Mishchenko, T. Georgiou, M. I. Katsnelson, L. Eaves, S. V. Morozov, N. M. R. Peres, J. Leist, A. K. Geim, K. S. Novoselov, L. A. Ponomarenko, *Science* **2012**, *335*, 947.
[67] Y. Hernandez, V. Nicolosi, M. Lotya, F. M. Blighe, Z. Sun, S. De, I. T. McGovern, B. Holland, M. Byrne, Y. K. Gun'Ko, J. J. Boland, P. Niraj, G. Duesberg, S. Krishnamurthy, R. Goodhue, J. Hutchison, V. Scardaci, A. C. Ferrari, J. N. Coleman, *Nat. Nanotechnol.* **2008**, *3*, 563.
[68] J. N. Coleman, M. Lotya, A. O'Neill, S. D. Bergin, P. J. King, U. Khan, K. Young, A. Gaucher, S. De, R. J. Smith, I. V. Shvets, S. K. Arora, G. Stanton, H.-Y. Kim, K. Lee, G. T. Kim, G. S. Duesberg, T. Hallam, J. J. Boland, J. J. Wang, J. F. Donegan, J. C. Grunlan, G. Moriarty, A. Shmeliov, R. J. Nicholls, J. M. Perkins, E. M. Grieveson, K. Theuwissen, D. W. McComb, P. D. Nellist, V. Nicolosi, *Science* **2011**, *331*, 568.
[69] C. Berger, Z. Song, T. Li, X. Li, A. Y. Ogbazghi, R. Feng, Z. Dai, A. N. Marchenkov, E. H. Conrad, P. N. First, W. A. de Heer, *J. Phys. Chem. B* **2004**, *108*, 19912.
[70] K. Nakatsuji, Y. Shibata, R. Niikura, F. Komori, K. Morita, S. Tanaka, *Phys. Rev. B* **2010**, *82*, 045428.
[71] J. Hass, W. A. de Heer, E. H. Conrad, *J. Phys. Condens. Matter* **2008**, *20*.
[72] K. V. Emtsev, F. Speck, T. Seyller, L. Ley, J. D. Riley, *Phys. Rev. B* **2008**, *77*, 155303.
[73] W. A. de Heer, C. Berger, X. Wu, P. N. First, E. H. Conrad, X. Li, T. Li, M. Sprinkle, J. Hass, M. L. Sadowski, M. Potemski, G. Martinez, *Solid State Commun.* **2007**, *143*, 92.
[74] J. Kedzierski, P. L. Hsu, P. Healey, P. W. Wyatt, C. L. Keast, M. Sprinkle, C. Berger, W. A. de Heer, *IEEE T. Electron Dev.* **2008**, *55*, 2078.
[75] J. S. Moon, D. Curtis, M. Hu, D. Wong, C. McGuire, P. M. Campbell, G. Jernigan, J. L. Tedesco, B. VanMil, R. Myers-Ward, C. Eddy, D. K. Gaskill, *Electron Device Lett. IEEE* **2009**, *30*, 650.
[76] Y.-M. Lin, C. Dimitrakopoulos, K. A. Jenkins, D. B. Farmer, H.-Y. Chiu, A. Grill, P. Avouris, *Science* **2010**, *327*, 662.
[77] Y. Zhu, S. Murali, W. Cai, X. Li, J. W. Suk, J. R. Potts, R. S. Ruoff, *Adv. Mater.* **2010**, *22*, 3906.
[78] X. S. Li, W. W. Cai, J. H. An, S. Kim, J. Nah, D. X. Yang, R. Piner, A. Velamakanni, I. Jung, E. Tutuc, S. K. Banerjee, L. Colombo, R. S. Ruoff, *Science* **2009**, *324*, 1312.
[79] Y. Yao, Z. Li, Z. Lin, K.-S. Moon, J. Agar, C. Wong, *J. Phys. Chem. C* **2011**, *115*, 5232.
[80] W. Gannett, W. Regan, K. Watanabe, T. Taniguchi, M. F. Crommie, A. Zettl, *Appl. Phys. Lett.* **2011**, *98*, 242105.
[81] M. P. Levendorf, C. S. Ruiz-Vargas, S. Garg, J. Park, *Nano Lett.* **2009**, *9*, 4479.
[82] M. Xu, D. Fujita, J. Gao, N. Hanagata, *ACS Nano* **2010**, *4*, 2937.
[83] T. Iwasaki, H. J. Park, M. Konuma, D. S. Lee, J. H. Smet, U. Starke, *Nano Lett.* **2010**, *11*, 79.
[84] S. Bae, H. Kim, Y. Lee, X. Xu, J.-S. Park, Y. Zheng, J. Balakrishnan, T. Lei, H. Ri Kim, Y. I. Song, Y.-J. Kim, K. S. Kim, B. Ozyilmaz, J.-H. Ahn, B. H. Hong, S. Iijima, *Nat. Nanotechnol.* **2010**, *5*, 574.
[85] Z. Sun, Z. Yan, J. Yao, E. Beitler, Y. Zhu, J. M. Tour, *Nature* **2010**, *468*, 549.
[86] A. W. RobertsonJ. H. Warner, *Nano Lett.* **2011**, *11*, 1182.
[87] M. S. Xu, D. Fujita, K. Sagisaka, E. Watanabe, N. Hanagata, *ACS Nano* **2011**, *5*, 1522.
[88] P. M. Ajayan, B. I. Yakobson, *Nat. Mater.* **2011**, *10*, 415.
[89] Q. Yu, L. A. Jauregui, W. Wu, R. Colby, J. Tian, Z. Su, H. Cao, Z. Liu, D. Pandey, D. Wei, T. F. Chung, P. Peng, N. P. Guisinger, E. A. Stach, J. Bao, S.-S. Pei, Y. P. Chen, *Nat. Mater.* **2011**, *10*, 443.
[90] P. Y. Huang, C. S. Ruiz-Vargas, A. M. van der Zande, W. S. Whitney, M. P. Levendorf, J. W. Kevek, S. Garg, J. S. Alden, C. J. Hustedt, Y. Zhu, J. Park, P. L. McEuen, D. A. Muller, *Nature* **2011**, *469*, 389.
[91] H. Wang, G. Wang, P. Bao, S. Yang, W. Zhu, X. Xie, W.-J. Zhang, *J. Am. Chem. Soc.* **2012**, *134*, 3627.
[92] A. Srivastava, C. Galande, L. Ci, L. Song, C. Rai, D. Jariwala, K. F. Kelly, P. M. Ajayan, *Chem. Mater.* **2010**, *22*, 3457.
[93] Z. Yan, Z. Peng, Z. Sun, J. Yao, Y. Zhu, Z. Liu, P. M. Ajayan, J. M. Tour, *ACS Nano* **2011**, *5*, 8187.
[94] H. Gullapalli, A. L. Mohana Reddy, S. Kilpatrick, M. Dubey, P. M. Ajayan, *Small* **2011**, *7*, 1697.
[95] A. L. M. Reddy, A. Srivastava, S. R. Gowda, H. Gullapalli, M. Dubey, P. M. Ajayan, *ACSNano* **2010**, *4*, 6337.
[96] F. Yavari, C. Kritzinger, C. Gaire, L. Song, H. Gulapalli, T. Borca-Tasciuc, P. M. Ajayan, N. Koratkar, *Small* **2010**, *6*, 2535.
[97] M. Y. Han, B. Özyilmaz, Y. Zhang, P. Kim, *Phys. Rev. Lett.* **2007**, *98*, 206805.
[98] J. Hu, X. Ruan, Y. P. Chen, *Nano Lett.* **2009**, *9*, 2730.
[99] J. Lu, P. S. E. Yeo, C. K. Gan, P. Wu, K. P. Loh, *Nat. Nanotechnol.* **2011**, *6*, 247.
[100] C. Volk, S. Fringes, B. Terrés, J. Dauber, S. Engels, S. Trellenkamp, C. Stampfer, *Nano Lett.* **2011**, *11*, 3581.
[101] J. Peng, W. Gao, B. K. Gupta, Z. Liu, R. Romero-Aburto, L. Ge, L. Song, L. B. Alemany, X. Zhan, G. Gao, S. A. Vithayathil, B. A. Kaipparettu, A. A. Marti, T. Hayashi, J.-J. Zhu, P. M. Ajayan, *Nano Lett.* **2012**, *12*, 844.
[102] H. Li, X. He, Z. Kang, H. Huang, Y. Liu, J. Liu, S. Lian, C. H. A. Tsang, X. Yang, S.-T. Lee, *Angew. Chem. Int. Ed.* **2010**, *49*, 4430.
[103] M. Bokdam, P. A. Khomyakov, G. Brocks, Z. Zhong, P. J. Kelly, *Nano Lett.* **2011**, *11*, 4631.
[104] L. Ci, L. Song, D. Jariwala, A. L. Elıas, W. Gao, M. Terrones, P. M. Ajayan, *Adv. Mater.* **2009**, *21*, 1
[105] D. Pan, J. Zhang, Z. Li, M. Wu, *Adv. Mater.* **2010**, *22*, 734.

[106] Y. Li, Y. Hu, Y. Zhao, G. Shi, L. Deng, Y. Hou, L. Qu, *Adv. Mater.* **2011**, *23*, 776.
[107] X. Yan, B. Li, X. Cui, Q. Wei, K. Tajima, L.-s. Li, *J. Phys. Chem. Lett.* **2011**, *2*, 1119.
[108] X. Yan, X. Cui, L.-s. Li, *J. Am. Chem. Soc.* **2010**, *132*, 5944.
[109] M. L. Mueller, X. Yan, J. A. McGuire, L.-s. Li, *Nano Lett.* **2010**, *10*, 2679.
[110] J. Liu, A. R. Wright, C. Zhang, Z. Ma, *Appl. Phys. Lett.* **2008**, *93*, 041106.
[111] A. R. Wright, J. C. Cao, C. Zhang, *Phys. Rev. Lett.* **2009**, *103*, 207401.
[112] F. Bonaccorso, Z. Sun, T. Hasan, A. C. Ferrari, *Nat Photon* **2010**, *4*, 611.
[113] J. H. LeeEduardo, K. Balasubramanian, R. T. Weitz, M. Burghard, K. Kern, *Nat. Nanotechnol.* **2008**, *3*, 486.
[114] X. Xu, N. M. Gabor, J. S. Alden, A. M. van der Zande, P. L. McEuen, *Nano Lett.* **2009**, *10*, 562.
[115] T. Mueller, F. Xia, P. Avouris, *Nat Photon* **2010**, *4*, 297.
[116] C. Stampfer, J. Güttinger, S. Hellmüller, F. Molitor, K. Ensslin, T. Ihn, *Phys. Rev. Lett.* **2009**, *102*, 056403.
[117] A. Bostwick, F. Speck, T. Seyller, K. Horn, M. Polini, R. Asgari, A. H. MacDonald, E. Rotenberg, *Science* **2010**, *328*, 999.
[118] F. Xia, T. Mueller, Y.-m. Lin, A. Valdes-Garcia, P. Avouris, *Nat. Nanotechnol.* **2009**, *4*, 839.
[119] F. Rana, *IEEE Trans. Nanotechnol.* **2008**, *7*, 91.
[120] V. Ryzhii, A. A. Dubinov, T. Otsuji, V. Mitin, M. S. Shur, *J. Appl. Phys.* **2010**, *107*, 054505.
[121] F. Xia, T. Mueller, R. Golizadeh-Mojarad, M. Freitag, Y.-m. Lin, J. Tsang, V. Perebeinos, P. Avouris, *Nano Lett.* **2009**, *9*, 1039.
[122] T. Mueller, F. Xia, M. Freitag, J. Tsang, P. Avouris, *Phys. Rev. B* **2009**, *79*, 245430.
[123] L. Prechtel, L. Song, D. Schuh, P. Ajayan, W. Wegscheider, A. W. Holleitner, *Nat Commun* **2012**, *3*, 646.
[124] J. F. Holzman, F. E. Vermeulen, A. Y. Elezzabi, *IEEE J. Quantum. Elect* **2000**, *36*, 130.
[125] J. Y. Dai, J. M. Yuan, P. Giannozzi, *Appl. Phys. Lett.* **2009**, *95*, 232105.
[126] B. D. Guo, Q. A. Liu, E. D. Chen, H. W. Zhu, L. A. Fang, J. R. Gong, *Nano Lett.* **2010**, *10*, 4975.
[127] Z. Jin, J. Yao, C. Kittrell, J. M. Tour, *ACS Nano* **2011**, *5*, 4112.
[128] U. A. Palnitkar, R. V. Kashid, M. A. More, D. S. Joag, L. S. Panchakarla, C. N. R. Rao, *Appl. Phys. Lett.* **2010**, *97*.
[129] W. Qian, X. Cui, R. Hao, Y. L. Hou, Z. Y. Zhang, *ACS Appl. Mater. Interfaces* **2011**, *3*, 2259.
[130] X. R. Wang, X. L. Li, L. Zhang, Y. Yoon, P. K. Weber, H. L. Wang, J. Guo, H. J. Dai, *Science* **2009**, *324*, 768.
[131] D. C. Wei, Y. Q. Liu, Y. Wang, H. L. Zhang, L. P. Huang, G. Yu, *Nano Lett.* **2009**, *9*, 1752.
[132] S. S. Yu, W. T. Zheng, C. Wang, Q. Jiang, *ACS Nano* **2010**, *4*, 7619.
[133] P. A. Denis, R. Faccio, A. W. Mombru, *ChemPhysChem* **2009**, *10*, 715.
[134] A. Q. Chen, Q. Y. Shao, L. Wang, F. Deng, *Sci. China Phys. Mech. Astron.* **2011**, *54*, 1438.
[135] A. Markevich, R. Jones, P. R. Briddon, *Phys. Rev. B* **2011**, *84*, 115439.
[136] R. R. Nair, W. Ren, R. Jalil, I. Riaz, V. G. Kravets, L. Britnell, P. Blake, F. Schedin, A. S. Mayorov, S. Yuan, M. I. Katsnelson, H.-M. Cheng, W. Strupinski, L. G. Bulusheva, A. V. Okotrub, I. V. Grigorieva, A. N. Grigorenko, K. S. Novoselov, A. K. Geim, *Small* **2010**, *6*, 2773.
[137] J. T. Robinson, J. S. Burgess, C. E. Junkermeier, S. C. Badescu, T. L. Reinecke, F. K. Perkins, M. K. Zalalutdniov, J. W. Baldwin, J. C. Culbertson, P. E. Sheehan, E. S. Snow, *Nano Lett.* **2010**, *10*, 3001.
[138] P. A. Denis, *J. Phys. Chem. C* **2011**, *115*, 13392.
[139] D. Lu, X. H. Yan, Y. Xiao, Y. R. Yang, *Phys. B Condens. Matter* **2011**, *406*, 4296.
[140] B. K. Gupta, P. Thanikaivelan, T. N. Narayanan, L. Song, W. Gao, T. Hayashi, A. Leela Mohana Reddy, A. Saha, V. Shanker, M. Endo, A. A. Martí, P. M. Ajayan, *Nano Lett.* **2011**, *11*, 5227.
[141] J. J. Yoo, K. Balakrishnan, J. Huang, V. Meunier, B. G. Sumpter, A. Srivastava, M. Conway, A. L. Mohana Reddy, J. Yu, R. Vajtai, P. M. Ajayan, *Nano Lett.* **2011**, *11*, 1423.
[142] W. Gao, N. Singh, L. Song, Z. Liu, A. L. M. Reddy, L. Ci, R. Vajtai, Q. Zhang, B. Wei, P. M. Ajayan, *Nat. Nanotechnol.* **2011**, *6*, 496.
[143] J. Taha-Tijerina, T. N. Narayanan, G. Gao, M. Rohde, D. A. Tsentalovich, M. Pasquali, P. M. Ajayan, *ACS Nano* **2012**, *6*, 1214.
[144] D. Pacile, J. C. Meyer, C. O. Girit, A. Zettl, *Appl. Phys. Lett.* **2008**, *92*, 133107.
[145] C. Y. Zhi, Y. Bando, C. C. Tang, H. Kuwahara, D. Golberg, *Adv. Mater.* **2009**, *21*, 2889.
[146] Z. Liu, L. Song, S. Zhao, J. Huang, L. Ma, J. Zhang, J. Lou, P. M. Ajayan, *Nano Lett.* **2011**, *11*, 2032.
[147] N. Alem, R. Erni, C. Kisielowski, M. D. Rossell, W. Gannett, A. Zettl, *Phys. Rev. B* **2009**, *80*, 155425.
[148] M. Wibbelt, H. Kohl, P. Kohler-Redlich, *Phys. Rev. B* **1999**, *59*, 11739.
[149] C. Jin, F. Lin, K. Suenaga, S. Iijima, *Phys. Rev. Lett.* **2009**, *102*, 195505.
[150] J. F. Moulder, W. F. Stickle, P. E. Sobol, D. Bombem, *Handbook of X-ray Photoeletron Spectroscopy*, Perkin Elmer Co., Eden Prairie, **1992**.
[151] K. S. Park, D. Y. Lee, K. J. Kim, D. W. Moon, *Appl. Phys. Lett.* **1997**, *70*, 315.
[152] R. Geick, C. H. Perry, G. Rupprecht, *Phys. Rev.* **1966**, *146*, 543.
[153] T. Kuzuba, Y. Sato, S. Yamaoka, K. Era, *Phys. Rev. B* **1978**, *18*, 4440.
[154] D. M. Hoffman, G. L. Doll, P. C. Eklund, *Phys. Rev. B* **1984**, *30*, 6051.
[155] C. Lee, X. Wei, J. W. Kysar, J. Hone, *Science* **2008**, *321*, 385.
[156] K. N. Kudin, G. E. Scuseria, B. I. Yakobson, *Phys. Rev. B* **2001**, *64*, 235406.
[157] L. Chun, B. Yoshio, Z. Chunyi, H. Yang, G. Dmitri, *Nanotechnology* **2009**, *20*, 385707.
[158] V. Eswaraiah, V. Sankaranarayanan, S. Ramaprabhu, *ACS Appl. Mater. Interfaces* **2011**, *3*, 4221.
[159] H. Xie, L. Chen, *J. Chem. Eng. Data* **2011**, *56*, 1030.
[160] A. A. Balandin, *Nat. Mater.* **2011**, *10*, 569.
[161] J. Yu, L. Qin, Y. Hao, S. Kuang, X. Bai, Y.-M. Chong, W. Zhang, E. Wang, *ACS Nano* **2010**, *4*, 414.
[162] T. T. Baby, R. Sundara, *J. Phys. Chem. C* **2011**, *115*, 8527.
[163] Y. Wei, X. Huaqing, B. Dan, *Nanotechnology* **2010**, *21*, 055705.
[164] T. T. Baby, S. Ramaprabhu, *J. Appl. Phys.* **2010**, *108*, 124308.
[165] S. S. Gupta, V. M. Siva, S. Krishnan, T. S. Sreeprasad, P. K. Singh, T. Pradeep, S. K. Das, *J. Appl. Phys.* **2011**, *110*, 084302.
[166] S. U. S. Choi, *J. Heat Transfer* **2009**, *131*, 033106.
[167] R. Larson, *The Structure and Rheology of Complex Fluids*, Oxford University Press, USA, **1998**.
[168] M. Terrones, A. Filho, A. Rao, *Doped Carbon Nanotubes: Synthesis, Characterization and Applications*, Vol. 111, Springer, Berlin **2008**, 531.
[169] O. Stephan, P. M. Ajayan, C. Colliex, P. Redlich, J. M. Lambert, P. Bernier, P. Lefin, *Science* **1994**, *266*, 1683.
[170] W. L. Wang, X. D. Bai, K. H. Liu, Z. Xu, D. Golberg, Y. Bando, E. G. wang, *J. Am. Chem. Soc.* **2006**, *128*, 6530.
[171] W. L. Wang, Y. Bando, C. Y. Zhi, W. Y. Fu, E. G. Wang, D. Golberg, *J. Am. Chem. Soc.* **2008**, *130*, 8144.
[172] Z. Xu, W. G. Lu, W. L. Wang, C. Z. Gu, K. H. Liu, X. D. Bai, E. G. Wang, H. J. Dai, *Adv. Mater.* **2008**, *20*, 3615.

[173] K. Raidongia, D. Jagadeesan, M. Upadhyay-Kahaly, U. V. Waghmare, S. K. Pati, M. Eswaramoorthy, C. N. R. Rao, *J. Mater, Chem.* **2008**, *18*, 83.
[174] K. Raidongia, A. Nag, K. P. S. S. Hembram, U. V. Waghmare, R. Datta, C. N. R. Rao, *Chem. Eur. J.* **2010**, *16*, 149.
[175] N. Kumar, K. S. Subrahmanyam, P. Chaturbedy, K. Raidongia, A. Govindaraj, K. P. S. S. Hembram, A. K. Mishra, U. V. Waghmare, C. N. R. Rao, *ChemSusChem* **2011**, *4*, 1662.
[176] N. Kumar, K. Raidongia, A. K. Mishra, U. V. Waghmare, A. Sundaresan, C. N. R. Rao, *J. Solid State Chem.* **2011**, *184*, 2902.
[177] J. H. Warner, M. H. Rümmeli, T. Gemming, B. Büchner, G. A. D. Briggs, *Nano Lett.* **2008**, *9*, 102.
[178] A. Zunger, A. Katzir, A. Halperin, *Phys. Rev. B* **1976**, *13*, 5560.
[179] W. Liu, Z. F. Wang, Q. W. Shi, J. Yang, F. Liu, *Phys. Rev. B* **2009**, *80*, 233405.
[180] R. Balog, B. Jorgensen, L. Nilsson, M. Andersen, E. Rienks, M. Bianchi, M. Fanetti, E. Laegsgaard, A. Baraldi, S. Lizzit, Z. Sljivancanin, F. Besenbacher, B. Hammer, T. G. Pedersen, P. Hofmann, L. Hornekaer, *Nat. Mater.* **2010**, *9*, 315
[181] arXiv:1105.1876.
[182] G. Gao, W. Gao, E. Cannuccia, J. Taha, L. Balicas, A. Mathkar, N. T. Narayanan, Z. Liu, B. K. Gupta, J. Peng, Y. Yin, A. Rubio, P. M. Ajayan, *Nano Lett.* **2012**, DOI: 10.1021/nl301061b.